National Research Council Canada
Conseil national de recherches Canada

NRC·CNRC

(2)

TRAJECTORIES AND STABILITY OF TRAILING VORTICES VERY NEAR THE GROUND

by

A.M. Drummond, R. Onno and B. Panneton

Institute for Aerospace Research

OTTAWA
DECEMBER 1991

AERONAUTICAL NOTE
IAR-AN-74
NRC NO. 32151

Canada

UNLIMITED
UNCLASSIFIED

INSTITUTE FOR AEROSPACE RESEARCH

SCIENTIFIC AND TECHNICAL PUBLICATIONS

AERONAUTICAL REPORTS

Aeronautical Reports (LR): Scientific and technical information pertaining to aeronautics considered important, complete, and a lasting contribution to existing knowledge.

Mechanical Engineering Reports (MS): Scientific and technical information pertaining to investigations outside aeronautics considered important, complete, and a lasting contribution to existing knowledge.

AERONAUTICAL NOTES (AN): Information less broad in scope but nevertheless of importance as a contribution to existing knowledge.

LABORATORY TECHNICAL REPORTS (LTR): Information receiving limited distribution because of preliminary data, security classification, proprietary, or other reasons.

Details on the availability of these publications may be obtained from:

Graphics Section,
National Research Council Canada,
Institute for Aerospace Research,
Bldg. M-16, Room 204,
Montreal Road,
Ottawa, Ontario
K1A 0R6

INSTITUT DE RECHERCHE AÉROSPATIALE

PUBLICATIONS SCIENTIFIQUES ET TECHNIQUES

RAPPORTS D'AÉRONAUTIQUE

Rapports d'aéronautique (LR): Informations scientifiques et techniques touchant l'aéronautique jugées importantes, complètes et durables en termes de contribution aux connaissances actuelles.

Rapports de génie mécanique (MS): Informations scientifiques et techniques sur la recherche externe à l'aéronautique jugées importantes, complètes et durables en termes de contribution aux connaissances actuelles.

CAHIERS D'AÉRONAUTIQUE (AN): Informations de moindre portée mais importantes en termes d'accroissement des connaissances.

RAPPORTS TECHNIQUES DE LABORATOIRE (LTR): Informations peu disséminées pour des raisons d'usage secret, de droit de propriété ou autres ou parce qu'elles constituent des données préliminaires.

Les publications ci-dessus peuvent être obtenues à l'adresse suivante:

Section des graphiques,
Conseil national de recherches Canada,
Institut de recherche aérospatiale,
Im. M-16, pièce 204,
Chemin de Montréal,
Ottawa (Ontario)
K1A 0R6

TRAJECTORIES AND STABILITY OF TRAILING VORTICES VERY NEAR THE GROUND

TRAJECTOIRES ET STABILITÉ DES VORTEX DE BOUT D'AILE À PROXIMITÉ DU SOL

by

A.M. Drummond, R. Onno and B. Panneton

Institute for Aerospace Research

OTTAWA
DECEMBER 1991

AERONAUTICAL NOTE
IAR-AN-74
NRC NO. 32151

S.R.M. Sinclair, Head/Chef
Flight Research Laboratory/
Laboratoire de recherches en vol

G.F. Marsters
Director General
Le directeur général

ABSTRACT

The behaviour of the trailing vortices of a Harvard aircraft used as the spraying vehicle during a set of experiments in aerial spraying over flat terrain for agricultural applications is discussed. The aircraft flew at a nominal altitude of 3 m (10 ft.) above ground at a speed of 56.7 m/s (110 knots). The stability and trajectory of a chosen element of the trailing vortices were measured by analyzing movie films taken by a ground-based camera and by a camera in a helicopter hovering at about 244 m (800 ft.) above the aircraft. The vortices decayed by core bursting in every case and the time to burst was usually in agreement with other published data for a light aircraft out of ground effect. The downwind vortex almost always burst before the upwind vortex and in most cases, both upwind and downwind vortices exhibited about the same amount of rebound even though the downwind vortex generally had a shorter lifetime. The classical inviscid theory for vortex descent was not a good model for the current experiments but it was able to predict with some success the lateral separation between the vortices when the aircraft wing tip height was arbitrarily reduced by a factor of 0.85. It was concluded that vortex core bursting and rebound must be included in any procedure for calculating aerial spray deposit on the ground.

RÉSUMÉ

Ce rapport présente des données expérimentales sur le comportement des vortex de bout d'aile pour un avoin Harvard. Le scénario expérimental reproduit les conditions d'arrosage aérien en agriculture sur un terrain plat. L'avion évoluait à 3 m au-dessus du sol et à une vitesse de 56.7 m/s. La stabilité de même que la trajectoire d'un élément des vortex ont été mesurées à partir de films provenant d'une caméra au sol et d'une caméra héliportée à une altitude de 244 m. Dans tous les cas, la désintégration des vortex survient par éclatement du coeur. Les temps écoulés entre la formation et la désintégration d'un élément de vortex obtenus lors de nos expériences sont en accord avec des données publiées précédemment pour un avion léger en l'absence d'un effet de sol. En général, le vortex situé sous le vent se désintègre en premier et plus rapidement. Malgré cela, les deux vortex rebondissent avec des amplitudes comparables. Les trajectoires expérimentales des vortex diffèrent grandement de celles obtenues à l'aide de la théorie basée sur les écoulements potentiels. Toutefois, l'écartement mesuré des vortex est prédit avec succès par la théorie en diminuant de façon arbitraire l'altitude initiale à 85% de sa valeur réelle. En conclusion, les données obtenues lors des expériences montrent que la désintégration des vortex par éclatement du coeur et le rebondissement des vortex sont deux phénomènes qui doivent être décris par des modèles de dispersion des gouttes en arrosage aérien.

TABLE OF CONTENTS

LIST OF SYMBOLS

b	a constant in the turbulent dissipation rate variation with height
C	height of ground-based camera
D	distance between helicopter markers
H	height of vortex above ground
K	empirical constant in the time to burst correlation
r	rebound height
t	time
T	time to start core bursting
TP,TS	time of end of experimental analysis for the port, starboard vortices
U	wind speed, 3 minute average
x	horizontal coordinate perpendicular to the sample line, origin at central helicopter marker
X	distance of vortex element in x direction
y	coordinate down the sample line, origin at central helicopter marker
Y	measurement of horizontal distance of vortex element from ideal aircraft path in the y direction, airborne camera
Y_c	distance from central helicopter marker to the ground-based camera
z	vertical coordinate, origin at central helicopter marker
Z	measurement of position of vortex element in z direction, ground-based camera
α	angle of average wind to the y axis
β	angle between aircraft flight path and x axis
γ	distance down y axis where aircraft path intersects the y axis
δ	distance in x direction of aircraft marker from the origin
θ	elevation angle of vortex above ground-based camera
ϵ	turbulent dissipation rate

LIST OF TABLES

LIST OF FIGURES

1.0 INTRODUCTION

The Institute for Aerospace Research (IAR) and Agriculture Canada cooperated in a joint research program on aerial spraying in agricultural applications during the summer and fall of 1989. A set of experiments was conducted to attempt the assessment of the roles of wing tip vortices and atmospheric turbulence on the downwind dispersion of spray droplets released from an aircraft. The parameters of the problem such as spray nozzles, terrain and aircraft height were chosen to simulate current practices in agriculture.

To support this research, a new spray deposit analysis system was developed (Refs. 1,2) and a new second generation sonic anemometer was created (Refs. 3,4). In addition, a new video system was installed in the helicopter associated with the experiments. However, a significant portion of the effort was an extension of and improvements to methods and systems developed at the Flight Research Laboratory (FRL) of IAR while simulating aerial spraying in forestry (Refs. 5,6).

The scope of this report is restricted to the discussion of the trajectories of the trailing vortices and their stability along with a measurement of the aircraft speed and altitude for each experiment. The meteorological aspects of the experiments such as the sonic anemometer installation and operation in the field, a critical assessment of anemometer performance and the wind data for each experiment have been reported (Ref. 4) while the results of spray deposit on the ground will be presented in another forum. Also, vertical profiles of spray concentration are in the process of being determined both by Agriculture Canada and by the Applied Aerodynamics Laboratory of IAR. In the final stage of this cooperative program, it is planned to attempt the correlation of experimentally determined ground deposition with some calculated results based on theory but using all of the available experimental evidence.

2.0 DESCRIPTION OF THE EXPERIMENTS

The same experimental strategy as reported in References 5 and 6 was employed by the spraying aircraft (Harvard) as it flew over the end of a spray deposit sample line with a helicopter (Bell 47) hovering above. The cores of the trailing vortices from each wing tip of the Harvard were marked by smoke and the resulting filaments were photographed both by a fixed, ground-based camera and by an airborne camera in the helicopter as the vortices moved down the spray sample line. The ground-based camera was a 16 mm Hycam running at a nominal 120 frames per second while the airborne camera was a 70 mm Vinten operating at 8 frames per second. Two parallel lines of Kromekote cards for sampling the spray deposition on the ground were laid out downwind from the aircraft flight line

while a meteorological system of three sonic anemometers recorded the atmospheric variables necessary to determine the mean wind profile, turbulence and atmospheric stability. These sonic anemometers were two of the new devices developed at the Flight Research Laboratory while the third was a commercial device that has been in service since 1985.

The spraying system of high pressure air, low pressure fluid tank, fluid flow regulation and spray boom installed in the Harvard aircraft were described in Reference 5 while the TeeJet 8005 nozzles were used in the current set of experiments to suit the drop size spectrum and flow rate appropriate to agricultural practices. As before, the spray fluid was ID585 with 2% Automate Red dye added to obtain sufficient contrast for analysis of the spray deposit samples. There was an additional component added to the spray fluid for gas chromatographic analysis of the drift samplers, 1 or 2% Tris (2-Ethyl-Hexyl) Phosphate or TEHP. The system of special, high-density smoke generators used to mark the vortex cores was developed over the years at the Flight Research Laboratory (Ref. 5).

Since aircraft height is a very important parameter in aerial spraying, the plan of the original research program was that experiments would be performed at two nominal heights over two seasons but delays in hardware development forced the cancellation of field work for the first season. Unfortunately, this resulted in a reduction in the number of experiments carried out and the cancellation of most of the flights at the higher of the two planned altitudes. All but one of the experiments was carried out at a nominal altitude of 3 m (10 ft.) with only the last flight being at 6.1 m (20 ft.). For all the experiments, an aircraft speed of 56.7 m/s (110 knots) was requested and in most cases the pilot was able to achieve this goal quite closely.

The 32.4 hectares (80 acre) experimental site was situated near Navan, Ont. in a region that was generally flat for at least 8 km in any direction. The same experimental site had been employed (Refs. 5,6) in previous years but a significant effort was expended on drainage for the current program so that an experiment could be undertaken when the meteorological conditions were correct without regard to previous rainfall. Two sets of two lines spaced 30 m apart and 250 m long (Fig. 1) used for deploying the spray samplers were oriented at 50 and 110 degrees magnetic, respectively. The sample line at 50 degrees was chosen to be in line with the predominant wind direction from the south-west in the summer months. The spray aircraft flew over a designated end of one of the sets of sample lines in the directions marked on the Figure as 'ideal a/c path'. The other direction was chosen so that the pilot could most easily set the correct speed and altitude on a flight line perpendicular to the sample line, considering the local obstructions from trees. For flights over the north-west corner, it was impossible for the aircraft to fly perpendicular to the sample

line because of a large grove of trees beyond the experimental area.

The designated end of a sample line was chosen on the basis of the direction of the mean wind as judged about a half an hour before the arrival of the aircraft, a sufficient time to set up the markers and spray sample cards. If the wind was predominantly from the south-west, say, with an angle between the mean wind and the spray sample line of no more than 30 degrees, then the designated end would be the south-west. Sometimes the wind shifted direction after the experiment was prepared and before the arrival of the aircraft resulting in a violation of the 30 degree wind angle limit.

The spray aircraft was guided to the end of the designated sample line by a movable red marker which also served as a central reference point in the field of view of the ground-based camera. For Flights 2 to 4, the marker was on the center of the 'ideal aircraft path' but the pilots had difficulty seeing it because the marker was necessarily close to the ground with the aircraft passing directly over it. To solve the visibility problem, the pilot was asked to fly between two taller markers, about 1.5 m wide by 1 m high, installed 7.6 m (25 ft.) either side of the 'ideal path' for Flights 5 to 13 inclusive. However, initial observations showed that the downwind marker appeared to influence the stability of the downwind vortex and so for the remaining Flights 14 to 22, one marker was placed 15.2 m (50 ft.) upwind of the 'ideal path' and another large marker was set on the 'ideal path' a long way past the sample line. The former marker became the camera reference while the latter was visible to the pilot and far enough away that the aircraft was pulling up from the spray run before passing over it. More will be said later about the influence of the marker on vortex stability (Sect. 5.2).

The helicopter pilot used a video camera to view a set of ground markers on a monitor in the cockpit as an aid in maintaining the correct position above the end of the sample line. These video pictures were also recorded as a back-up to the airborne camera. On Figure 1, the circular symbols represent the ground markers for the video system while the cross-hatched square symbols show the locations of the ground-based camera. Figure 2 shows the detailed dimensions of each of the sample lines extending from the ground-based camera location to the aircraft path. The camera station is 51 m past center field and 176 m from the aircraft flight line while the distance between the helicopter markers (D) varied for each of the sample line ends nominally named south-west, north-west, north-east and south-east.

The fields of view of the airborne photographic and video cameras were somewhat different, the former being approximately one third larger than the latter. Thus, it was quite possible for the helicopter to move its hover point sufficiently that some of the

video display would be lost while the Vinten camera was recording good data. The width of the field of view of the ground-based camera was approximately 41.1 m, while that of the airborne camera was about 137.2 m for the helicopter hovering at 240 m above ground level.

Figures 3 and 4 show the Harvard aircraft from frames taken by the ground-based and airborne cameras respectively for Flight 22. On Figure 3, the spray and the smoke-marked vortices are clearly visible as is the aircraft marker. Figure 4 shows the helicopter markers (large white squares), the two spray sample lines and the spray sample cards (small white dots). It is hard to discern the aircraft marker here on the print from the movie film although the projection system allowed an easy identification of the marker. Figures 5 and 6 show typical views of the vortex trails from the ground-based and airborne cameras respectively after the aircraft has left both fields of view.

In all, 22 flights were performed over the period from June to October, 1989. Table 1 shows the date of each flight, the time in the morning that the aircraft passed over the sample line, which camera was functioning and which anemometer was able to contribute a 3 minute average. Flight 1 is not shown because it was considered to be a test of the experimental protocol.

The ground-based camera did not function for Flights 16 and 17 while the airborne camera was not working properly for Flights 3,4,12,15,16 and 19. The video system did not record useable material for Flights 3,4,12 and 16. Malfunction of the Vinten was usually caused by an improperly mounted film cassette on the body of the camera while poor video records were usually caused by the position of the helicopter.

Five flights (Flts. 3,4,12,16 and 17) are marked by an asterisk which means that the vortex trajectory cannot be recovered either because of a total failure of the airborne devices or because of no vortex height measurement due to a faulty Hycam camera. The vortex trajectories for Flights 15 and 19 were salvaged by using the video tape instead of the Vinten film. No further reference will be made to the marked Flights in the rest of the discussion on vortex trajectories though stability data was available from the video tapes in all cases.

Table 2 shows data concerning the aircraft flight path (Fig. 7) and it lists for each flight the corner the aircraft flew over, the aircraft speed and altitude (see Sect. 3.0), the offset distance γ (positive down the sample line) where the aircraft path crossed the sample line and the angular deviation β from perpendicularity of the flight path to the sample line. The distance between the ground-based camera marker and the center helicopter marker δ is in the next column followed by an indication of the aircraft marker location. The relative placement of the

aircraft and central helicopter markers δ is of fundamental importance in the spatial synchronization of the two film media while β and γ are necessary to determine the initial positions of the vortices.

The 3 minute averages of wind speed and direction starting at the time the aircraft passed over the sample line were reliably obtained by the FRL sonic anemometer at the 9.1 m level (SSA2) while the FRL sonic anemometer at the 20.1 m level (SSA1) failed for Flights 11 and 12 only. The commercial sonic anemometer (CSA) at the 4.5 m level failed to provide useful 3 minute averages for the last four flights. Table 3 lists the wind speed and direction with respect to the chosen sample line.

3.0 AIRCRAFT SPEED AND ALTITUDE

The aircraft speed and altitude were obtained from analysis of the films recorded by the ground-based camera. A print of one such frame is shown in Figure 3. The position of the aircraft in the field of view was determined by the location of the propeller spinner, a point on the aircraft that was easy to identify with some precision on every film given the various conditions of lighting experienced during the experimental program.

From a projection of the Hycam film onto a sheet of white paper, the first and last positions of the aircraft were marked on the paper along with the number of frames. The distance travelled between these positions is converted into feet by using the length scale obtained from the ratio between the real Harvard length (8.8 m, 29 feet) and the length of the projected airplane image at the aircraft marker. The frame rate appropriate to when the aircraft is in view is obtained by counting the number of frames between images of light pulses on the edge of the film at 0.100 second intervals emitted by a subsidiary pulse generator. Thus, the aircraft speed is calculated using the number of frames and frame rate along with the measured distance travelled. The aircraft height is obtained relative to the bottom of the aircraft marker with the aircraft over the marker using the previously determined length scale.

This procedure of determining aircraft speed yields the speed of the aircraft with respect to fixed axes on the ground and no account is taken here of the aircraft speed with respect to the air. Table 2 lists the aircraft speed with respect to the ground in knots and the altitude in meters for all the flights.

4.0 VORTEX TRAJECTORY

The trajectories of the upwind and downwind vortices from a flight were separately determined as plots of height H above ground versus distance Y down the spray sample line, time being an implicit variable along the path. In the next few paragraphs, a

short description of the procedures used to obtain the trajectories will be given.

4.1 Film Reading and Creation of the Raw Data Files

The films from both cameras were separately projected onto the same white sheet of paper fixed to the palette of a Scriptel model SPD-1212T digitizer. Considering the projections from the two cameras in turn such as those shown on Figures 5 and 6, a mouse was used to send the coordinate of a point on the image of a vortex to a PC computer. Because of the different frame rates of the two media, careful synchronization of the frame counters of the films had to be performed using the aircraft marker, the only point visible on both films. When the aircraft was seen to pass over that point, that frame from both projectors was used to establish a common time origin.

After moving the films forward in each projector by the correct number of frames accounting for the different frame rates, both vortices in both images were projected at the same time. Following a sequential protocol regarding which vortex from which camera was being recorded, a sufficient number of points along the vortices were digitized to trace the images across the entire field of view of both cameras to form the raw data files in 'digitizer' units. The centres of the helicopter markers were digitized on each Vinten frame in order to maintain a length scale (using the dimension D, Fig. 2) and orientation which was necessitated because the helicopter moved vertically and laterally between frames in its attempt to remain stationary over the markers. Conversely, the length scale for the fixed Hycam was established only once when the Harvard was over the aircraft marker. The vortices were usually not continuous trails across the film because of vortex instability (Sect. 5.2) and a method to indicate breaks in the smoke trails was incorporated in the data file.

4.2 Creating the Data Files in Real units

The raw data files in 'digitizer' units were processed into the form of real distance units relative to an appropriate origin for each camera. For the ground-based camera, the origin was the bottom of the aircraft marker with vertical distance Z positive up and horizontal distance X positive from left to right as determined by an observer at the camera. The determination of X and Z relied on the scale that had already been determined from the speed and altitude calculations. For the airborne camera, the origin was the center helicopter marker with distance Y positive down the sample line toward the ground-based camera and X positive from left to right in the same sense as the ground-based camera. The distances Y and X were measured using the scale determined by the dimension D per frame. The relevant geometry is shown on Figure 7.

Because of the sinuous motion of the vortices and because the vortex instability caused breaks in the smoke trails, it was necessary to follow the life of the same element of vorticity in generating the vortex trajectories for each flight. It was assumed that a given element of the vortex would translate at a steady rate in the x direction under the action of the mean x component of wind. Knowing the time interval between frames being analyzed (Δt), the x coordinate of the vortex element being followed was calculated by

$$X = X_0 + U \sin \alpha \, \Delta t$$

and the values of Z and Y were taken at that value of X. The sign of α, the angle between the wind and the sample line, is positive for counter-clockwise rotation about the z axis following the right hand rule.

Table 3 lists the average wind speed and direction from a 3 minute time period commencing when the aircraft passed over the aircraft marker. An initial position X_0 was arbitrarily chosen to be at the aircraft marker because that was the center of the field of view of the Hycam, the smaller of the two fields of view. Of course, with the entire field of view of both cameras being digitized, it would be a simple task to repeat the calculations with a different choice of X_0. A discussion concerning that point will be presented later (Sect. 5.7).

4.3 The Trajectory

The geometry for determining the H-Y coordinate of the element of the vortex is given on Figure 8. H_0 and Z_0 are the initial vortex heights and measurements of vortex position by the Hycam using the scale determined by the aircraft dimension on the centre line while H and Z are the corresponding values at a later time. H is determined by:

$$\begin{aligned} H &= Z - h \\ &= Z - Y \tan \Theta \\ &= Z(1-Y/Y_c) + C\, Y/Y_c \end{aligned}$$

5.0 RESULTS

5.1 Vortex Trajectories

The vortex trajectories for Flights 2 to 22 are shown on Figures 9 to 24 as graphs of height H versus distance down the sample line Y. The initial position of each vortex is taken to be at the wing tip at 6.4 m (21 ft.) either side of the real aircraft track at the aircraft height (Table 2). The symbols represent

experimental points at various times, usually at 0.5 second intervals and the adjacent solid line running close to the data is the result of applying a box-car filter (Sect. 5.4) to the experimental data in an attempt to obtain smoother trajectories. Each vortex is identified as 'P' for port (circular symbols) or 'S' for starboard (square symbols) while the dash-dot line is a representation of the aircraft wing. The dotted lines are the trajectories of vortices from the classical, inviscid model (see Sect. 5.5) translating down the sample line at a rate determined by the y component of the mean wind (Table 3) and the mutually induced velocities from the vortices. The initial point for the dotted line is the theoretical position of the fully rolled up vortex at $\pi/4$ of the semi-span. The triangular symbol on both of the theoretical trajectory lines is placed at the earliest extinction time of the two vortices while the lines are continued to the maximum time of experimental analysis.

In the data box at the lower right of each figure, the starting point of the analysis (X_0) is noted along with the times in seconds when the measurements ended for each vortex, TS or TP for the starboard or port vortices. The notation 'BURST' is applied (see Sect. 5.2) if that vortex suffered core bursting instability at the vortex element being followed causing the end of the experimental analysis for that vortex. Depending upon the choice of the initial element, it is possible that this message may not appear even if the vortex ultimately suffered core bursting at a different place along its length.

5.2 Vortex Stability

Both vortices suffered core bursting instability in every case with the downwind vortex generally bursting earlier. The commencement time for core bursting, the onset of axial flow in the vortex, was obtained by examination of the airborne camera film (like Fig. 6). The film was advanced until the first break in the smoke trail marking the core was observed and then the film was reversed until the aircraft was at the same place, the number of frames moved being recorded as a measure of the age of the vortex. Unfortunately, no independent measure of the frame rate was available for the Vinten camera and reliance had to be placed on the frame rate selected by a switch on the camera. The process of film analysis was then repeated for the other member of the pair.

The growth rate of the break in the vortex core is a measure of the strength of the axial flow directed in both directions away from the initial break point. The strength of this flow varied somewhat from flight to flight but it was always strong and dominated the local flow.

Though the mechanism of core bursting is not well understood (Refs. 7,16 for example), experimental correlations of the time to burst have been made (Refs. 5,8) using the turbulent dissipation

rate ϵ to the 1/3 power. Tombach et al. (Ref. 9) have also constructed a model of the core bursting process where the time to burst is an inverse function of $\epsilon^{1/3}$. In Ref. 4, the turbulent dissipation rate was obtained for each anemometer for every experiment using the power spectral density of turbulence in the mean wind direction, the mean wind speed and the mean square turbulence intensity. Since ϵ is a hyperbolic function of height (ϵ*H = b, Ref. 17), the value of 'b' for each experiment was obtained by a least squares hyperbolic fit to the measurements of ϵ from anemometers at 20.1 m and at 9.1 m. Thus, the turbulent dissipation rate was calculated using this value of 'b' and the aircraft height (Table 2). For Flights 11 and 12 when SSA1 malfunctioned, ϵ was taken from SSA2 only. Table 4 lists the times to burst for the port and starboard vortices along with the values of ϵ from the two sonic anemometers. The notation 'D' denotes which vortex of the pair was the downwind member.

Remembering the earlier discussion that the aircraft markers downwind of the aircraft path appeared to affect vortex stability for Flights 5 to 13 inclusive, the downwind vortices for these flights suffered their first core bursting right at the marker except for Flights 5 and 11. In these two cases, the downwind vortex experienced a burst a short time before it reached the marker but then, each vortex burst again as it passed over the marker. The marker-vortex interaction could not be seen on the video tape for Flight 12 because the helicopter had moved after the Harvard had passed over the marker. There were no obvious effects of the marker on the upwind vortex.

Figure 25 shows the results of time to burst versus the turbulent dissipation rate to the 1/3 power for all of the flights from 2 to 22, except Flight 17, which was excluded because the turbulent dissipation rate was not accurately computed in that case. Time to burst data was available from the video tapes even if the Vinten camera did not function. On the Figure, upwind and downwind vortices from the port wing tip are noted by squares and crossed squares respectively while circles serve the same purpose for the starboard vortex. Vertical lines connecting the points help to identify a vortex pair for any flight.

The experimental correlations of time to burst with the turbulent dissipation rate based on the model of Tombach et al. (Ref. 9) are of the form:

$$T = \frac{K}{\epsilon^{1/3}}$$

where the constant K in the formula is related to the wing span of the aircraft.

On Figure 25, the dashed lines labelled 'K = 70' and 'K = 15' are the upper and lower boundaries (Ref. 8) of time to burst data for a small aircraft out of ground effect. It appears that those lines are appropriate boundaries in the present case except when the bursting process was initiated for flights where vortex interaction with the downwind aircraft marker triggered the bursting. Those data are noted by the flight number beside the symbols for purposes of identification. The dotted line marked K = 10 is drawn as the line providing a lower bound to all of the data for these experiments and 5 out of the 6 flights with this early trigger are between this line and the lower boundary from Tombach.

In a recent paper, Khorrami (Ref. 15) found two new modes of viscous instability in a trailing vortex, one symmetric and one asymmetric. He proceeded to cast doubt upon the conventional explanation of core bursting because he argued that the disturbances were travelling outside the core leaving the core intact. He calculated the radial distribution of energy in the unstable modes and he concluded that most of the energy was distributed outside the vortex core. Pictures of aircraft contrails at high altitude (10,000 m) were then presented where core bursting and Crow instability were coexistent and he used the images to support his analysis. However, Khorrami suggested that more research will be required before his comments could be taken beyond the current stage of speculation. It is not clear how the ground effect enters into the study of viscous instability.

5.3 Vortex Rebound

In most cases, either the upwind or downwind vortex or both vortices experienced a rebound with the size of the excursions being about equally distributed between the two vortices even though the downwind vortex usually had a shorter life. Thus, when the downwind vortex did rebound, the rebound tended to be more energetic. The consistent rebound of the upwind vortex has not previously been reported though the rebounding behaviour of the downwind vortex has been thoroughly discussed in both experimental and theoretical frameworks (Refs. 5,10-13). In Reference 5, the data showed that the upwind vortex had a very small rebound in only two out of 24 flights during the simulation of forestry spraying using the same aircraft. In that work, the aircraft altitude was considerably higher (5.5 m to 19.2 m or 18 to 63 feet) than in the current simulation of spraying in agriculture.

For the present set of experiments, Table 5 illustrates the extent of the rebound and the main results from that Table are summarized here as the number of flights within the indicated rebound height ranges. Here, a rebound of height r is defined as the amount of rebound greater than or equal to (r-1) and less than r following the minimum point of the trajectory.

REBOUND HEIGHT r m	UPWIND VORTEX	DOWNWIND VORTEX
= 0 none	3	3
< .6 small	2	4
.6 < 1.5 moderate	6	3
1.5 < 2.4 large	5	6

From examination of Table 5, the amount of rebound is larger when the lifetime of the vortex is longer for both the upwind and downwind vortices indicating that vortex stability ultimately controls the amount of rebound.

With the aircraft very close to the ground in these experiments, the location of the maximum velocity at the edge of the core of the upwind vortex is also very close to the ground and this velocity can overpower the crosswind causing a separated boundary layer to be induced beneath it. Thus, one would expect the cases of 'none' and 'small' rebound for the upwind vortex to correlate well with a large crosswind velocity. This did indeed happen because the 3 minute average wind speed was greater than 3.0 m/s for all these flights while it was generally lower for all other classes of rebound. The only contradiction is that the crosswind speed was 3.8 m/s for Flight 19 where a large rebound occurred.

5.4 Smoothing the Measured Trajectories

In an attempt to smooth the measured vortex trajectories, two techniques were applied. The first method used was a 'B-spline' routine resident in the graphics package used to plot the trajectories but this method failed to converge, resulting in an even worse representation of the vortex path. Then, a simpler 'box-car filter' was applied where the filtered i'th data point has height and downwind distance coordinates that are the linear averages of the coordinates of the i'th data point and the two adjacent points at (i-1) and (i+1). The first and last data points are not filtered.

Examining the filtered trajectories for Flights 14 and 22, for example, the benefit of using a smoothing technique is shown because the physically improbable jagged nature of the measured path, especially on the upwind vortex, has been removed in both cases while the characteristic rebound has been preserved.

5.5 Inviscid Theory

The classical treatment of the descent of a pair of ideal,

two-dimensional vortices toward a solid ground plane in inviscid flow has been reported in many places (Refs. 10,14 for example). In the absence of any crosswind, the vortices descend under the mutually induced velocities of the two vortices and their images in a coordinate system that is fixed to the ground. The trajectories of the upwind and downwind vortices are mirror images of each other as they descend vertically while they separate and translate laterally at the same speed in opposite directions. Crosswind can be added as a coordinate transformation by algebraically adding an amount $U\Delta t$ to the lateral distance moved by each vortex.

The theoretical vortex trajectories based on this model were computed for each experiment using the measured aircraft speed and aircraft height as the initial vertical position of the vortex along with the component of the 3 minute average wind down the sample line for the coordinate transformation. The aircraft weight was taken to be 2490 kg. (5400 pounds) for all experiments. The dotted lines denoted 'THEORY' on Figures 9 to 24 are the results of the computations. After examination of the figures, it is clear that these theoretical results do not compare well with the measured trajectories and application of the model as a predictive tool for vortex trajectory work would supply meaningless results. A similar conclusion was reached in Ref. 5.

The lateral separation distance between the vortices was observed to increase with time in general agreement with the motion predicted by the classical inviscid theory. This behaviour was not observed in the forestry simulation experiments (Ref. 5), perhaps because of the higher aircraft altitude where the lateral separation velocities are expected to be much lower. In the present case however, the comparison between the experimentally determined and theoretically predicted lateral separation of the vortices was surprisingly accurate when the height of the aircraft for the theory was arbitrarily taken to be 0.85 of the measured aircraft height. This comparison was valid only while both vortices were present in the experimental trajectories. The factor 0.85 was selected to increase the level of agreement and the choice has no basis in theory or in experiment.

The theory represents the wing as a line vortex with two trailing vortices initially all at the same height, a configuration which of course does not allow for the dihedral of the wing on the real aircraft. For the Harvard, the dihedral angle is 5 degrees and 41 minutes resulting in the wing root being 0.64 m (2.1 ft.) lower than the wing tip. The aircraft height was taken to be the height of the propeller spinner above the ground which is approximately the same as the wing tip. Thus, the average height of the lifting wing is less than that quoted for the aircraft and the factor 0.85 quoted above is about the right order of magnitude to account for this effect.

Figures 26 and 27 show two good comparisons between the best-fit line to the experimental data and the inviscid theory while Figure 28 shows the worst comparison. At each experimental data point, the square of the difference between the predicted and measured separation was computed and summed over all the data points to obtain a root mean square deviation of the theory from experiment. An RMS value less than about 1 1/2 meters is considered to indicate a good comparison and, after examining the data in Table 6 for all the experiments, it is seen that 11 out of the 16 flights satisfied this criterion. The flights with the largest RMS errors, Flights 11,21 and 22, all had aircraft speeds below 51.5 m/s (100 knots) though it is not known why this correlation should occur.

5.6 Average Vortex Trajectories

An alternative point of view to the following of a single vortex element in the construction of a vortex trajectory is to follow ten, say, different elements equally spaced along the aircraft flight path and average their coordinates to obtain an average trajectory. One problem that arises in this procedure is that a vortex burst occurring at a certain place on the visible vortex trail will not be experienced by all of the elements forming the average until the burst has dissipated the entire trail. Thus, one might expect differences between average and single element trajectories to appear predominantly in the downwind vortex as it would exhibit a longer lifetime on average with more motion.

Trajectories for ten elements were averaged for 11 out of the 16 flights. Flights over the northwest corner were not processed (Flts. 7,8,13 and 15) because the offset and angle of the flight path to the ideal direction caused different initial positions for each element along the vortex. If the results for the first 11 computations warranted it, the program could be modified to account for variations in the initial conditions of the elements. Flight 19, with the Y data being taken from the video, did not have the same spatial extent and thus it was not possible to have the same element spacing as in the other cases perhaps causing an unfair comparison of the methods.

The following table illustrates the differences between average and single element trajectories for the downwind vortices. There were no significant differences in the trajectories for the upwind vortices.

DIFFERENCES	FLIGHT NUMBERS
NONE	5,11,21,22
SMALL DOWNWIND	2,6,9,14,18,20
LARGE DOWNWIND	10

The table shows that there is no real advantage to the average trajectory over the single element trajectory. In fact, the single element trajectory is to be preferred because it follows as accurately as possible the movement of the burst which is the predominant factor in determining the latter stages of the vortex life. The computation of average trajectories for flights over the northwest corner does not appear to be necessary.

5.7 Implications of Results for Aerial Spraying

The results presented in this report show that real physical effects such as vortex rebound and instability that are not accounted for in classical theories dominate the behaviour of the vortices. In any modelling work purported to apply to agricultural application, an inclusion of at least an approximate treatment of these phenomena should be made. For example, since the vortex dominates the initial spray behaviour, it is expected that quite wide variations in ground deposit along the aircraft path should be expected as a result of vortex core bursting. The strong axial flow observed to take place in either direction away from the point of core bursting could serve to collect the spray between points of instability. Khorrami's speculations tend to support this because he has calculated a surprisingly large axial flow velocity outside the core for an unstable mode, the region where most of the spray is located.

An additional perplexing issue is that after the burst, the state of the vortex is not even qualitatively understood. In at least one instance (Flight 21), there was considerable downwind transport (125 m) of 'a slice' of the smoke marking the core after core bursting had occurred and the slice was observed to retain significant rotation. Perhaps in this case some of the flow external to the core was destroyed leaving the core to persist. The implication for spray deposit is that even though bursting had occurred, spray transport by the vortex was still possible, at least for the smaller drops.

Vortex descent and rebound significantly change the effective height of spray release from that of the aircraft resulting in a large expected variation in downwind deposit density even with the same wind speed. Without a reasonable physical explanation of this phenomenon, models designed to predict spray deposit density cannot be expected to supply accurate results.

6.0 CONCLUSIONS

Trajectories of selected elements of aircraft trailing vortices and their stability have been presented in this report for fifteen flights at a nominal aircraft speed of 56.7 m/s (110 knots) at an altitude of 3 m above ground with the sixteenth occurring at 6.1 m. The actual aircraft speed and altitude were also obtained for each flight.

The trajectories were obtained by analysis of movie films from both a ground-based and an airborne camera though a video tape replaced the airborne camera film in two cases. A single element of the vortex was followed by using the wind component along the aircraft flight path to adjust the point of measurement.

Both the upwind and downwind vortices were observed to decay by core bursting in every case with the downwind vortex usually bursting first. Correlations of time to burst with data from other light aircraft out of ground effect indicated that the vortices in the present set of experiments behaved in the same general manner except when the aircraft marker was downwind. In that case, the interaction of the downwind vortex and the marker caused core bursting to occur even more quickly as though the marker triggered the event.

The trajectories of both the upwind and downwind vortices exhibited rebound in most cases with both vortices exhibiting about the same amount of rebound even though the lifetime of the downwind vortex was generally shorter. The rebound of the upwind vortex was reduced by a strong crosswind.

In general, the experimental results (measurements) were not well modelled by the classical inviscid theory. However, the lateral separation between vortices was very well predicted when the aircraft height was reduced by an arbitrary factor of 0.85 for the calculations. It was conjectured that the factor was a result of the aircraft dihedral placing the average height of the wing closer to the ground.

The implications of the results of this report on aerial spray behaviour were discussed and it was concluded that the effects of vortex core bursting and rebound on the motion of spray droplets must be included in calculations of ground deposition.

7.0 REFERENCES

1. Panneton, B. and Drummond, A.M., 'Digital Image Analysis of Spray Samples', Applied Engineering in Agriculture, Vol. 7, No. 2, pp. 273-278, 1991.

2. Panneton, B. and Drummond, A.M., 'A System for the Digital Image Analysis of Spray Samples', NRC IAR-AN-68, Nov., 1990.

3. Panneton, B., Drummond, A.M. and Barszczewski, A., 'Wind Tunnel Calibration of the FRL Sonic Anemometers', in review.

4. Drummond, A.M., Panneton, B. and Barszczewski, A., 'Meteorological Data from Agriculture Canada and the IAR Cooperative Experiments in Aerial Spraying', in review.

5. Drummond, A.M., Hamman, G. and Gauvin, R., 'Some Measurements on Vortex Descent and Stability Near the Ground', NRC LTR-FR-102, Sept., 1987.

6. Drummond, A.M., 'Some Experimental Results of Ground Deposition from Aerial Spraying', NRC LTR-FR-112, Sept., 1990.

7. Leibovich, S., 'Vortex Stability and Breakdown - Survey and Extension', AIAA Jrnl., Vol. 22, No. 9, Sept., 1984.

8. Tombach, I., 'Observations of Atmospheric Effects on the Transport and Decay of Trailing Vortex Wakes', AIAA Paper 73-110, Jan., 1973.

9. Tombach, I., Lissaman, P.B.S., Mullen, J.B. and Barker, S.J., 'Aircraft Vortex Wake Decay Near the Ground', FAA-RD-77-46, May, 1977.

10. Dee, F.W. and Nicholas, O.P., 'Flight Measurements of Wing-Tip Vortex Motion Near the Ground', RAE CP. No. 1065, Jan., 1968.

11. Harvey, J.K. and Perry, F.J., 'Flow Field Produced by Trailing Vortices in the Vicinity of the Ground', AIAA Jrnl., Vol. 9, No. 8, pp. 1659-1660, Aug., 1971.

12. Walker, J.D.A., 'The Boundary Layer Due to Rectilinear Vortex', Proc. Roy. Soc. Lond. a, Vol. 359, pp. 167-188, 1978.

13. Orlandi, P., 'Vortex Dipole Rebound from a Wall', Phys. Fluids A, Vol. 2, No. 8, pp. 1429-1436, Aug., 1990.

14. Lamb, H., 'Hydrodynamics', Cambridge University Press, 6th

Edn., 1932.

15. Khorrami, M.R., 'On the Viscous Modes of Instability of a Trailing Vortex', J. Fluid Mech., Vol. 225, pp. 197-212, 1991.

16. Escudier, M., 'Vortex Breakdown: Observations and Explanations', Progress in the Aerospace Sciences, Vol. 25, pp. 189-229, 1988.

17. Lissaman, P.B.S., Crow S.C., MacCready, P.B. Jr., Tombach, I.H. and Bate, E.R. Jr., 'Aircraft Vortex Wake Descent Under Real Atmospheric Effects', FAA-RD-73-120, Oct., 1973.

8.0 ACKNOWLEDGEMENTS

The creativity of Mr. Onno in devising the data acquisition program for digitizing the vortices, performing the laborious task of actually digitizing all the films and editing the data is gratefully acknowledged. The aircrew of the Flight Research Laboratory performed the low level flying task extremely well as can be seen by the aircraft height data in the text. The instrumentation was ably installed and repaired by Mr. W. Budarick and the experimental site was well maintained under the supervision of Mr. W.E. Slack. All these efforts contributed to the successful conclusion of the program.

TABLE 1

FLIGHT TIME AND INSTRUMENT OPERATING STATUS

FLT. NO.	DATE OF EXPT.	TIME OF SPRAY a.m.	CAMERA FUNCTIONING			METEOROLOGY 3 MIN.AVG.		
			HYCAM	VINTEN	VIDEO	SSA1	SSA2	CSA
2	Jun.22	8:20	yes	yes	yes	yes	yes	yes
3*	Jun.22	9:46	yes	no	no	yes	yes	yes
4*	Jul. 6	8:47	yes	no	no	yes	yes	yes
5	Jul.18	7:15	yes	yes	yes	yes	yes	yes
6	Jul.18	8:00	yes	yes	yes	yes	yes	yes
7	Jul.19	7:10	yes	yes	yes	yes	yes	yes
8	Jul.19	7:51	yes	yes	yes	yes	yes	yes
9	Jul.20	7:16	yes	yes	yes	yes	yes	yes
10	Jul.20	7:52	yes	yes	yes	yes	yes	yes
11	Jul.25	7:09	yes	yes	yes	no	yes	yes
12*	Jul.25	8:10	yes	no	no	no	yes	yes
13	Jul.26	7:38	yes	yes	yes	yes	yes	yes
14	Aug.10	9:16	yes	yes	yes	yes	yes	yes
15	Aug.17	7:48	yes	no	yes	yes	yes	yes
16*	Aug.24	7:35	no	no	no	yes	yes	yes
17*	Aug.24	8:07	no	yes	yes	yes	yes	yes
18	Sep.22	11:14	yes	yes	yes	yes	yes	yes
19	Oct.13	8:43	yes	no	yes	yes	yes	no
20	Oct.13	9:28	yes	yes	yes	yes	yes	no
21	Oct.24	8:34	yes	yes	yes	yes	yes	no
22	Oct.24	9:14	yes	yes	yes	yes	yes	no

'*' beside the Flight Number means the vortex trajectory cannot be analyzed.

TABLE 2

AIRCRAFT FLIGHT AND MARKER DATA

FLT. NO.	FLIGHT OVER CORNER	AIRCRAFT				MARKER	
		SPEED knots	HEIGHT m	γ OFFSET m	β ANGLE deg.	δ DIST. m	LOC'N see below
2	SE	108.5	3.3	0	0	-2.7	1
5	SW	107.5	3.8	1.6	0	-11.8	2
6	SW	105.3	4.1	1.6	0	-13.3	2
7	NW	108.6	3.7	0	8.1	-18.7	2
8	NW	108.1	3.7	0	12.4	-18.3	2
9	NE	109.9	3.4	0	0	0	2
10	NE	113.4	3.4	0	0	0	2
11	SW	98.0	3.6	-0.8	0	0	2
13	NW	115.8	3.4	-1.7	12.8	0	2
14	SW	107.3	3.9	-1.5	0	0	3
15	NW	101.5	3.9	8.5	11.0	0	3
18	SE	110.0	3.6	1.4	0	0	3
19	SW	110.5	3.4	0	0	0	3
20	SW	110.1	3.5	1.1	0	0	3
21	SW	93.7	2.8	1.6	0	0	3
22	SW	89.8	7.5	0.8	0	0	3

Aircraft Marker Location :

1 = 1 marker, at the center of the ideal aircraft track
2 = 2 markers, 7.6 m either side of ideal aircraft track
3 = 1 marker, 15.2 m upwind of ideal aircraft track

TABLE 3

METEOROLOGICAL DATA : 3 MINUTE AVERAGES
OBTAINED FROM ANEMOMETERS AT 9.1 m AND CSA At 4.5 m

FLT. NO.	WIND SPEED m/s	α SWATH ANGLE degrees
2	2.12	-20.0
5	0.41	33.1
6	2.98	-1.3
7	1.14	-3.0
8	2.04	17.2
9	1.32	3.1
10	3.96	-7.8
11	0.53	-55.3
13	2.85	27.1
14	2.14	-25.6
15	4.10	-39.8
18	1.34	1.6
19	3.81 #	-14.1
20	5.07 #	-27.5
21	2.36 #	5.4
22	4.06 #	-4.6

'#' beside the wind speed means that only SSA2 was used for this experiment due to CSA failure.

TABLE 4

TIME TO BURST AND TURBULENT DISSIPATION RATE

FLT. NO.	TIME TO BURST		TURB. DISS. RATE ϵ $cm^2 sec^{-3}$ (Ref.4)	
	PORT sec.	STARBOARD sec.	SSA1 20.1 m	SSA2 9.1 m
2	4 1/8 D	6 1/2	15	18
3	6 D	9	20	34
4	10	6 D	12	17
5	8 5/8	7 3/8 D	8	7
6	6 5/8	3 3/8 D	18	22
7	7 1/2	4 D	4	5
8	5 5/8	3 1/8 D	8	9
9	4 5/8 D	8	10	16
10	2 3/4 D	7	29	40
11	7 3/8	10 1/4 D	3*	3
12	8 1/2	6 D	11*	11
13	5 3/4	3 7/8 D	13	17
14	10 1/8	4 5/8 D	19	28
15	2 1/2	3 1/2 D	105	171
16	8 3/4	7 1/4 D	58	53
18	7 1/2 D	11 7/8	16	15
19	11	7 D	51	64
20	5	3 3/8 D	58	83
21	12	6 3/4 D	19	14
22	7 1/4	6 D	42	49

'*' means data for SSA1 copied from SSA2
'D' means vortex downwind

TABLE 5

REBOUND HEIGHT AND VORTEX LIFETIME

FLT. NO.	UPWIND VORTEX		DOWNWIND VORTEX	
	REBOUND HEIGHT LESS THAN r ft.	TIME sec.	REBOUND HEIGHT LESS THAN r ft.	TIME sec.
2	3	9	6	7
5	5	10.5	4	8
6	NONE	8.5	3	3.5
7	6	10.5	2	4
8	6	11	1	3
9	5	10.5	3	5.5
10	2	10.5	NONE	2.5
11	6	10.5	6	11.5
13	4	11	NONE	4
14	4	10	6	7.5
15	NONE	4	1	4
18	7	15	6	8.5
19	6	10.5	NONE	4.5
20	1	5	8	4
21	4	8.5	7	8.5
22	NONE	8	2	8

TABLE 6

LATERAL SEPARATION :
ROOT MEAN SQUARE DIFFERENCE BETWEEN THE
EXPERIMENTAL DATA AND THE INVISCID MODEL

FLT. NO.	RMS DIFFERENCE m
2	2.08
5	.57
6	1.00
7	.58
8	.97
9	.53
10	.73
11	3.18
13	.87
14	.80
15	1.03
18	.69
19	.23
20	1.74
21	8.98
22	7.80

note - aircraft height is 0.85 of real height for the theory

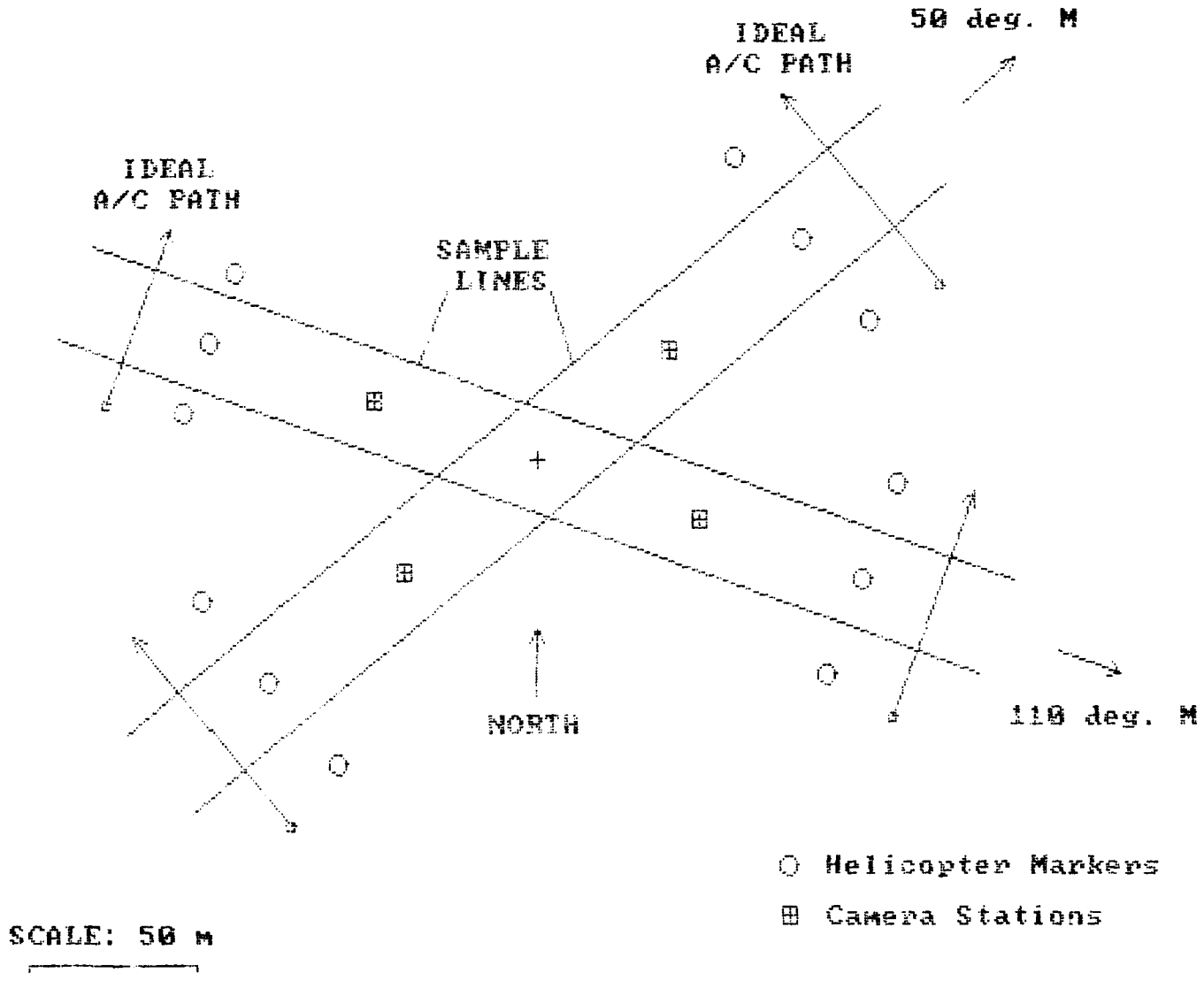

FIG. 1: THE EXPERIMENTAL SITE

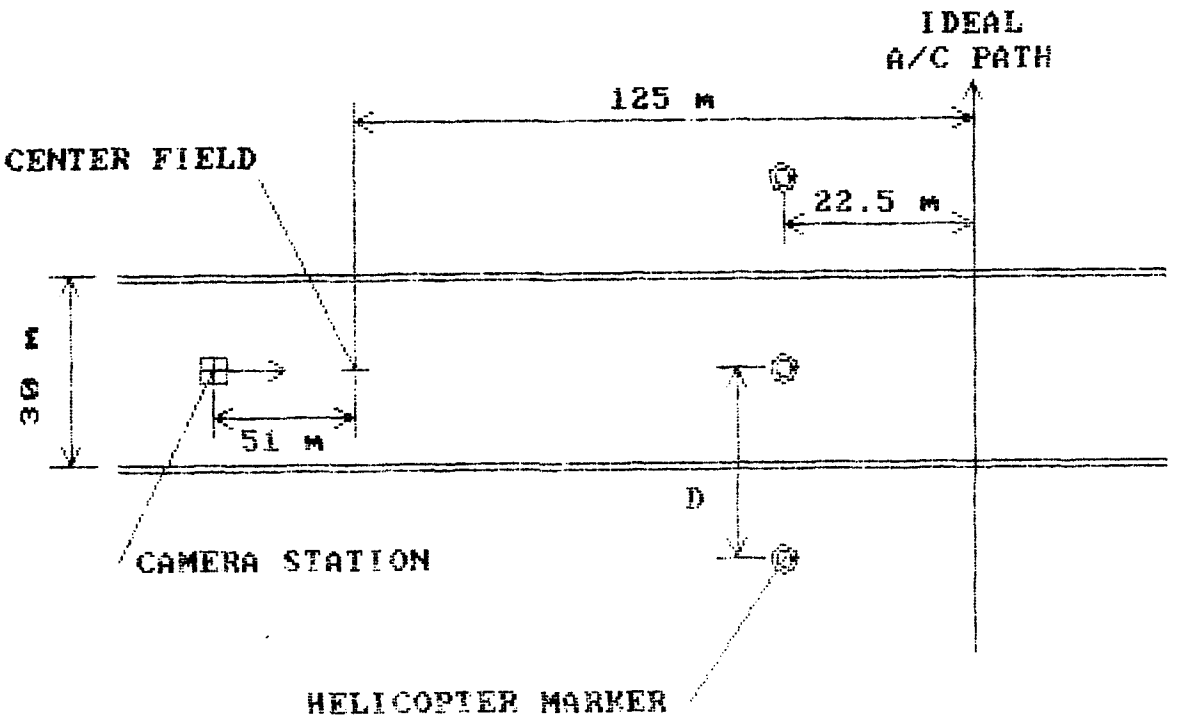

SWATH END	D m
SW	31.4
NW	22.5
NE	31.4
SE	30.5

FIG. 2: DIMENSIONS OF THE SITE

FIG. 3: THE HARVARD AIRCRAFT AS VIEWED BY THE GROUND-BASED CAMERA, FLT. 22

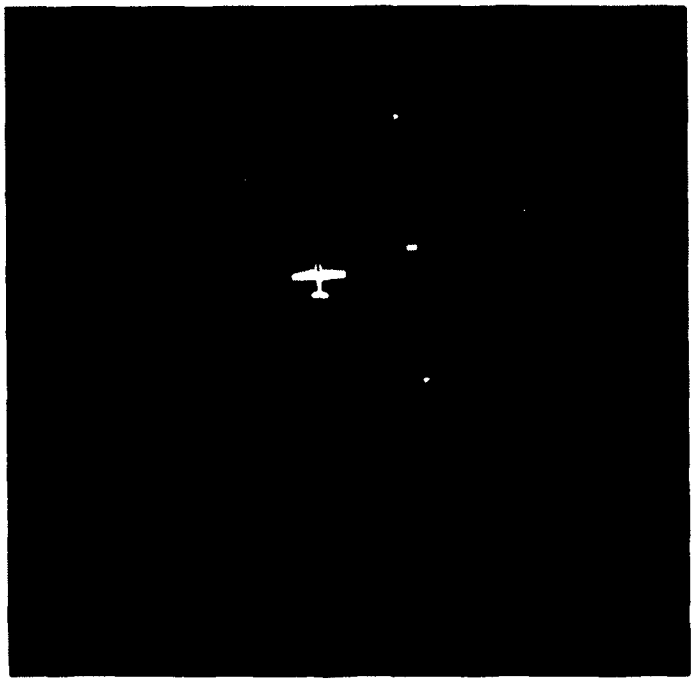

FIG. 4: THE HARVARD AIRCRAFT AS VIEWED BY THE AIRBORNE CAMERA, FLT. 22

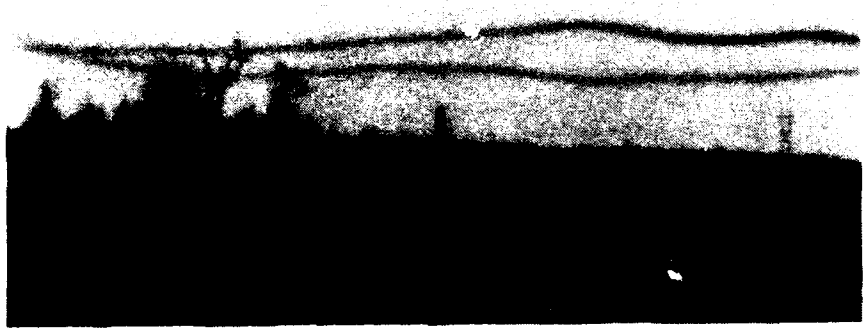

FIG. 5: VORTEX TRAILS AS VIEWED BY THE GROUND BASED CAMERA, FLT. 22

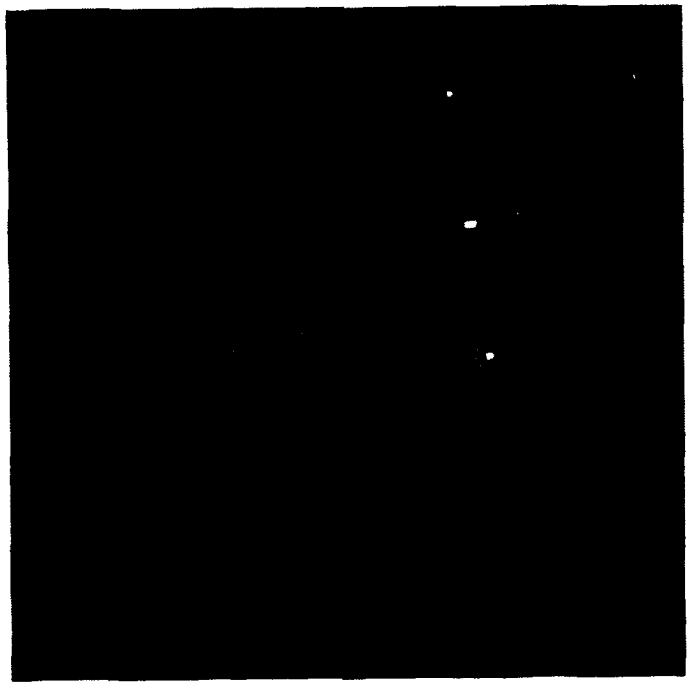

FIG. 6: VORTEX TRAILS AS VIEWED BY THE AIRBORNE CAMERA, FLT. 22

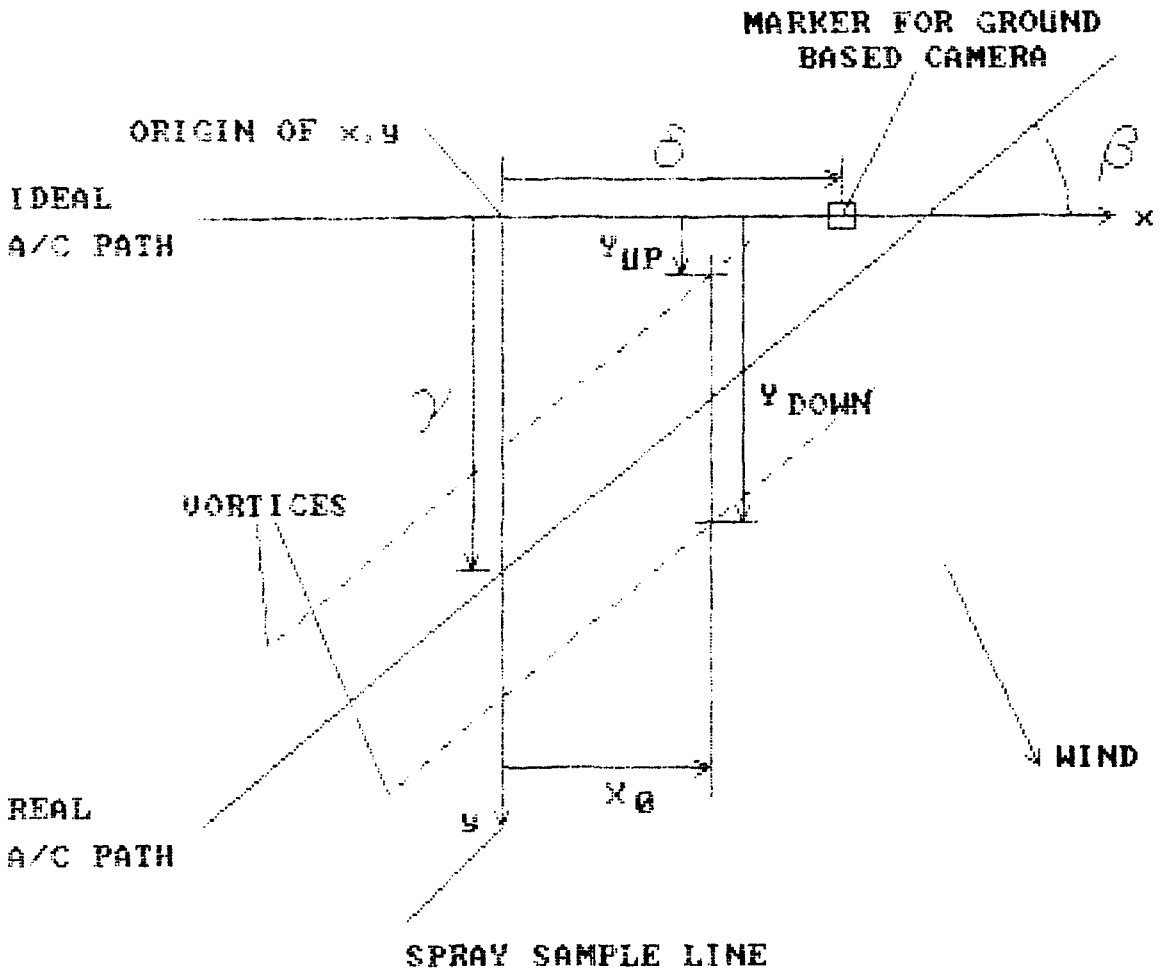

FIG. 7: GEOMETRY FOR VORTEX TRANSLATION

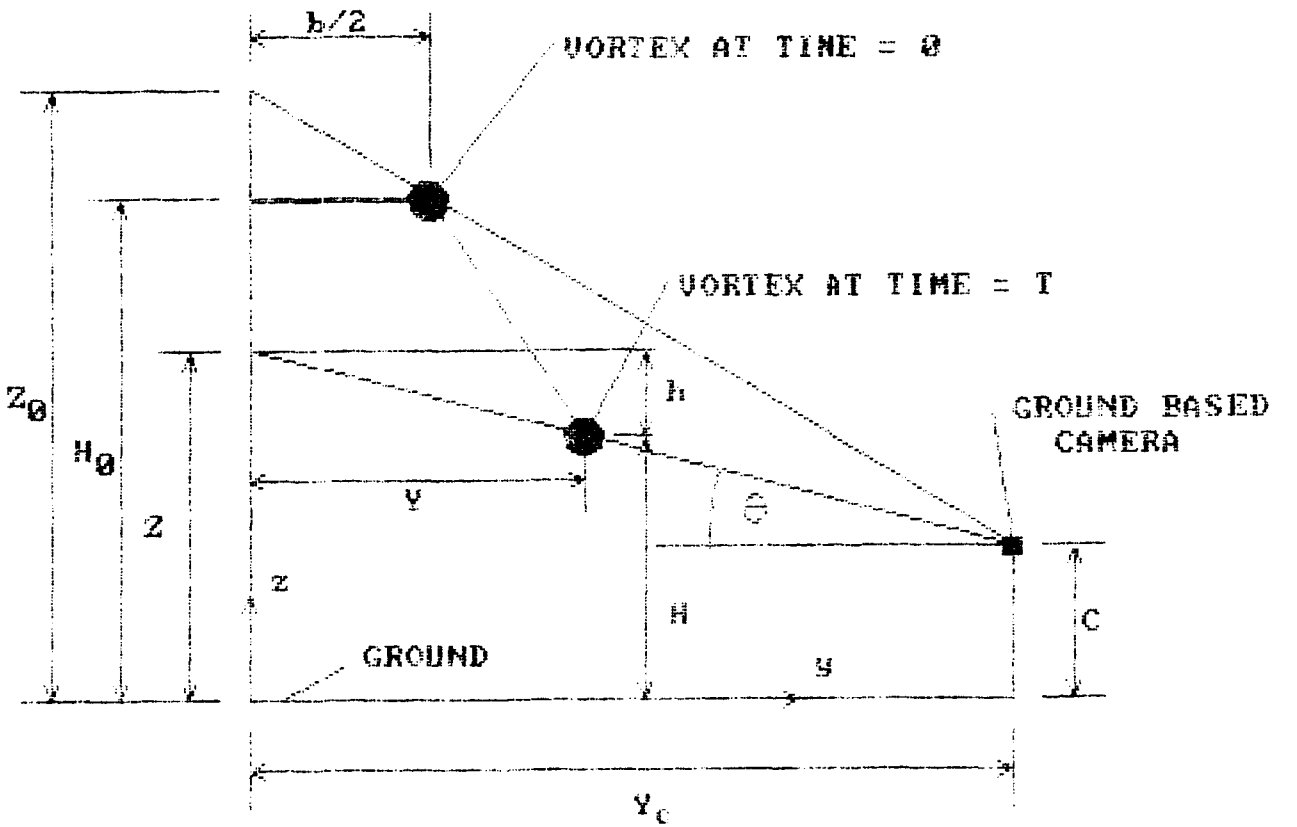

FIG. 8: GEOMETRY FOR VORTEX DECENT ANALYSIS

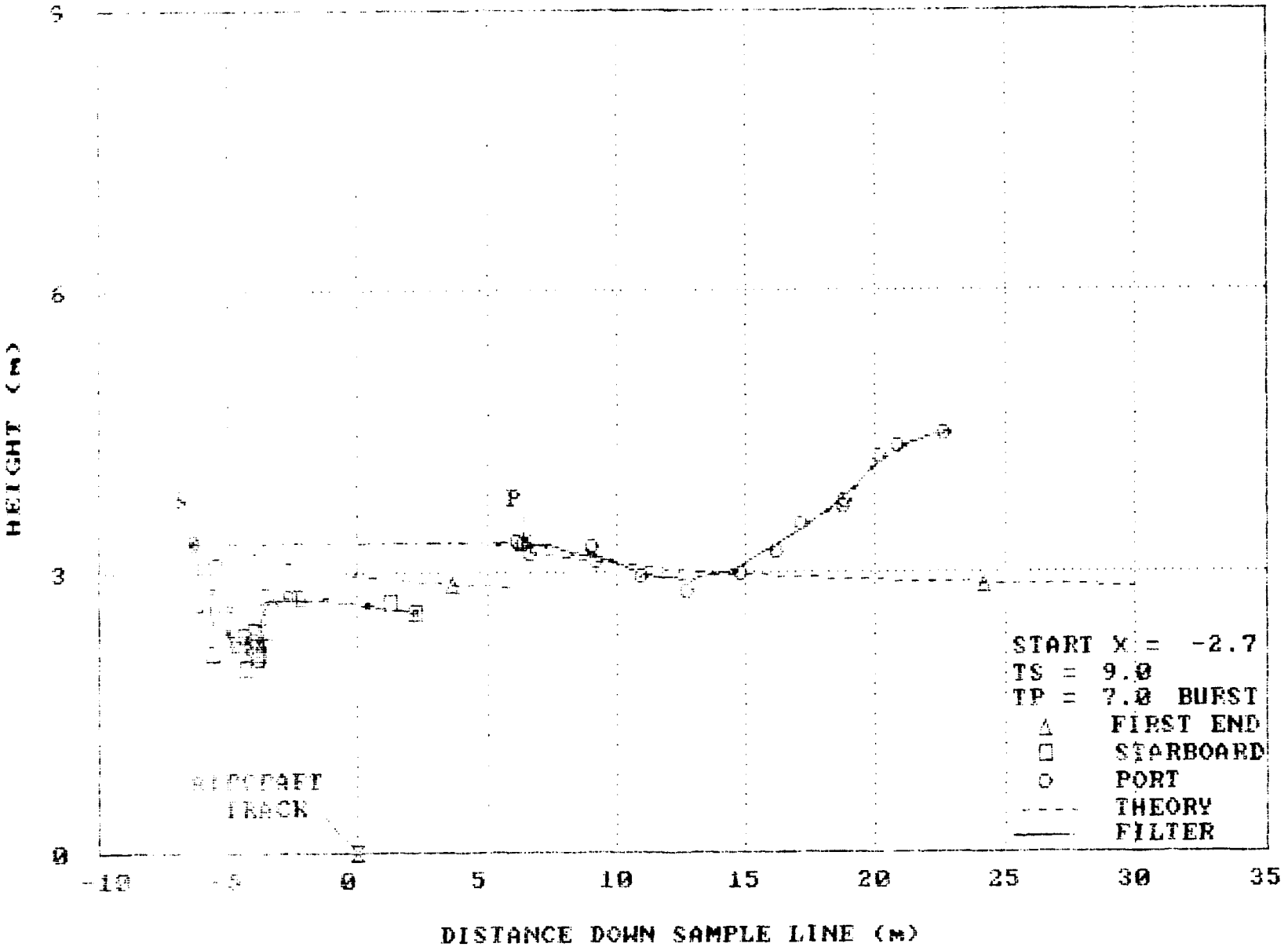

FIG. 9: VORTEX TRAJECTORY FOR FLT. 2

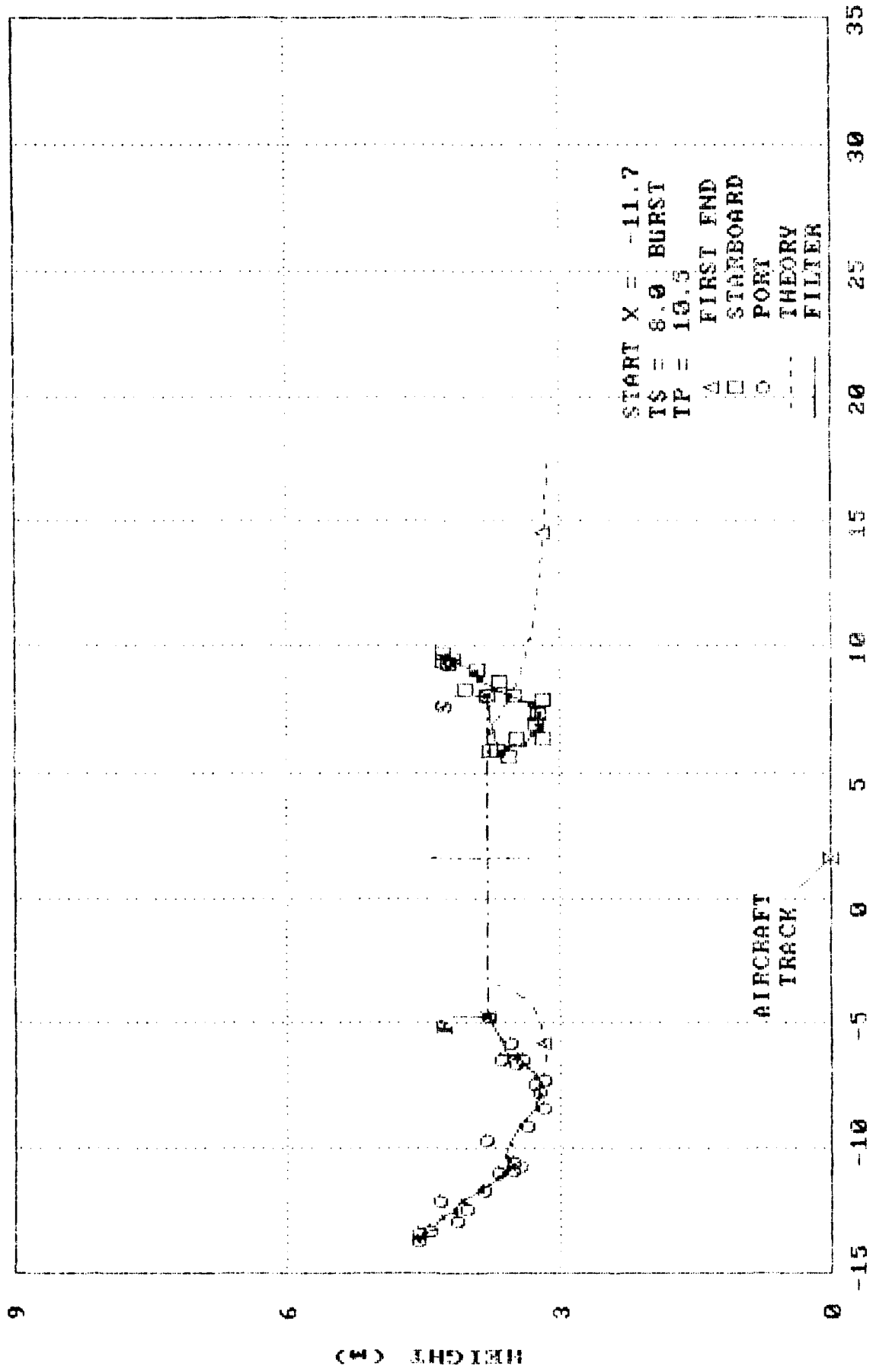

FIG. 10: VORTEX TRAJECTORY FOR FLT. 5

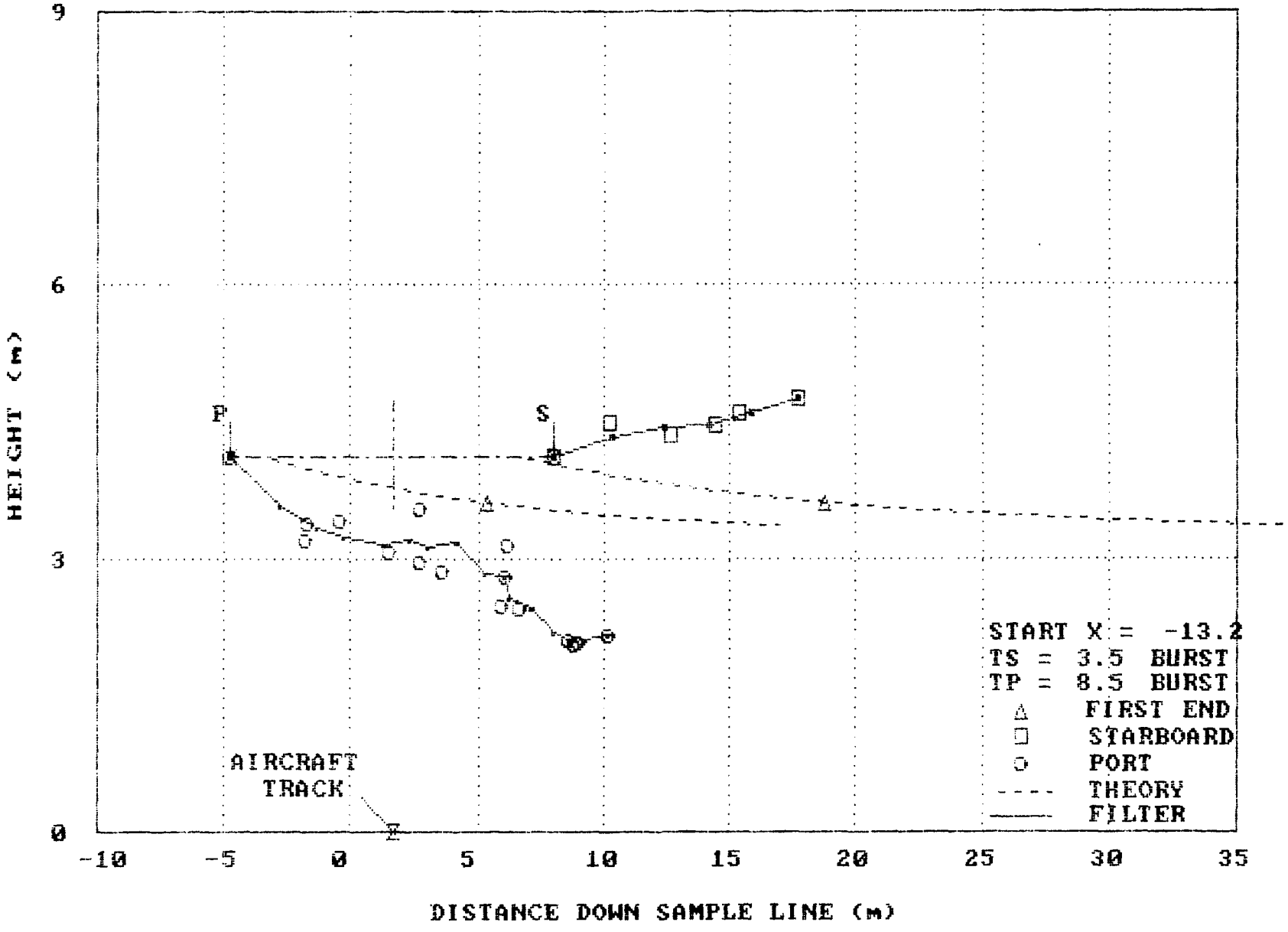

FIG. 11: VORTEX TRAJECTORY FOR FLT. 6

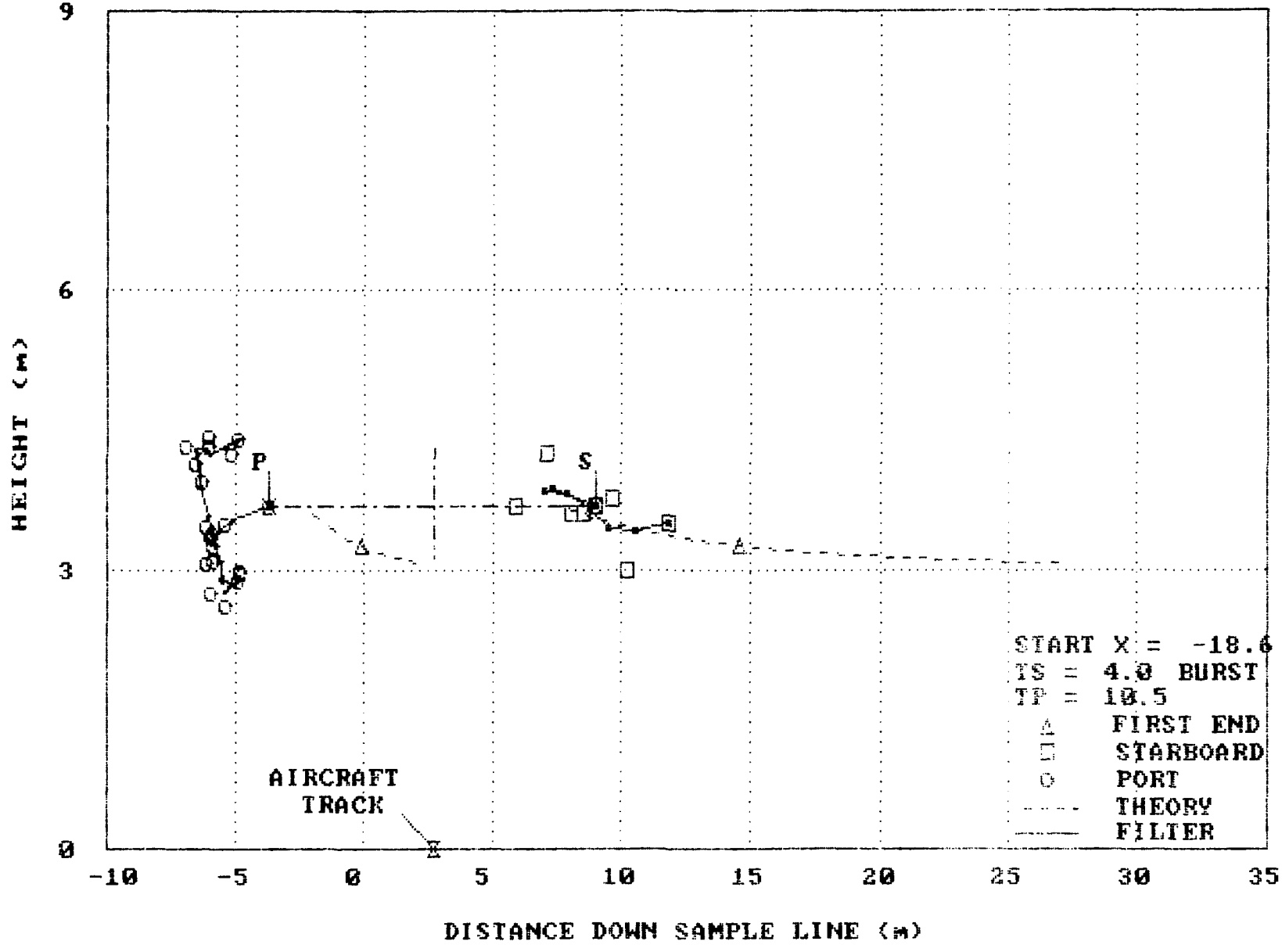

FIG. 12: VORTEX TRAJECTORY FOR FLT. 7

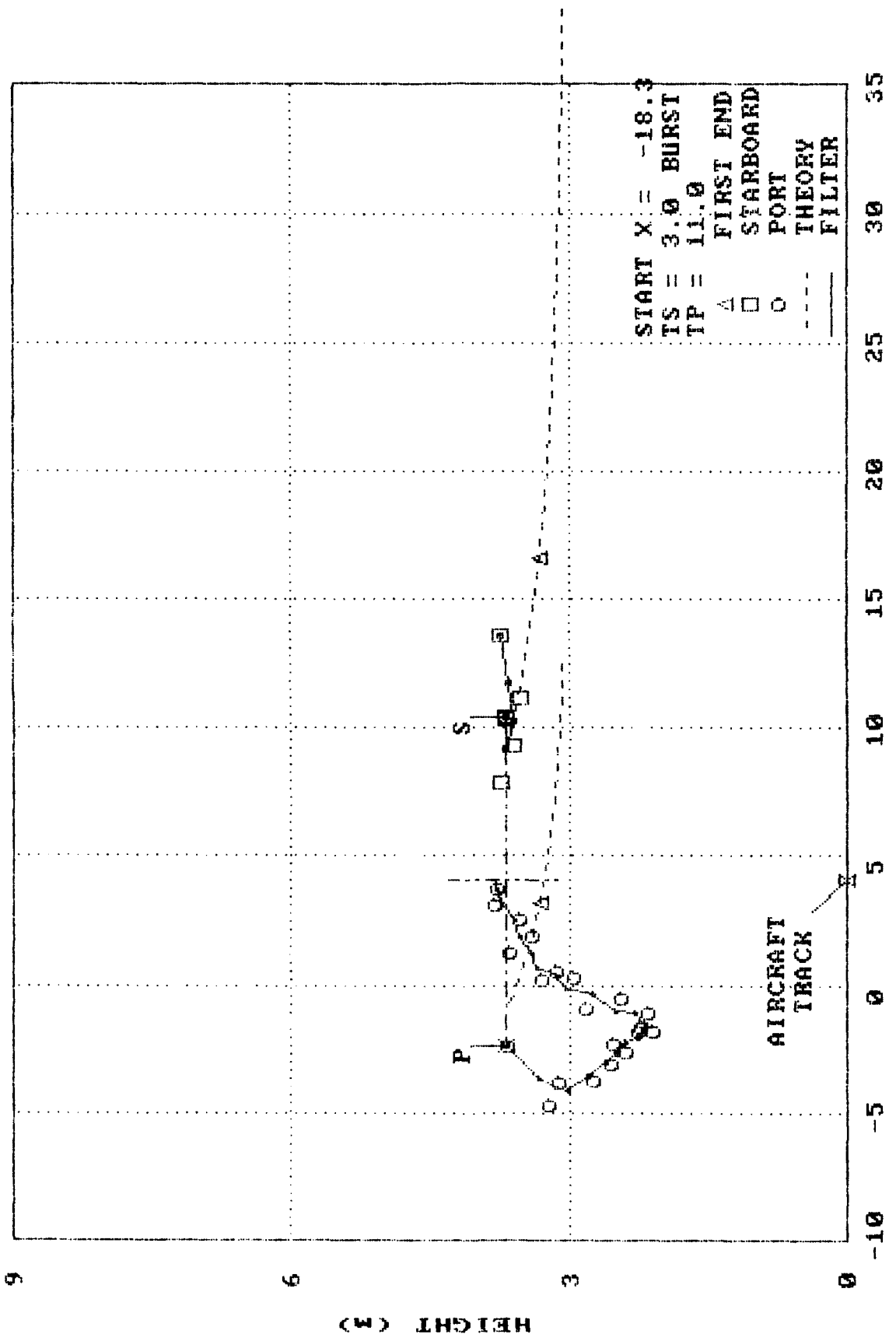

FIG. 13: VORTEX TRAJECTORY FOR FLT. 8

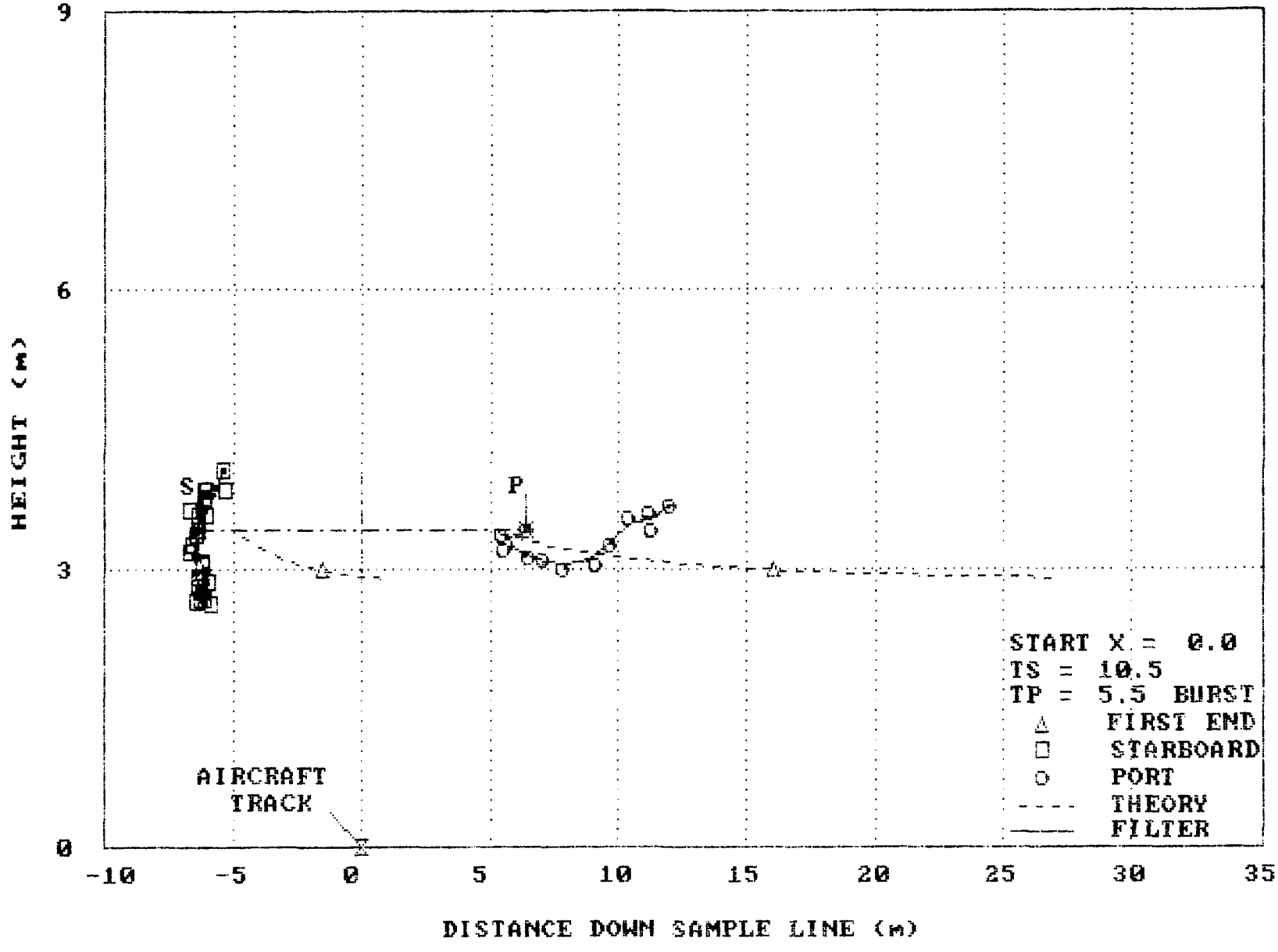

FIG. 14: VORTEX TRAJECTORY FOR FLT. 9

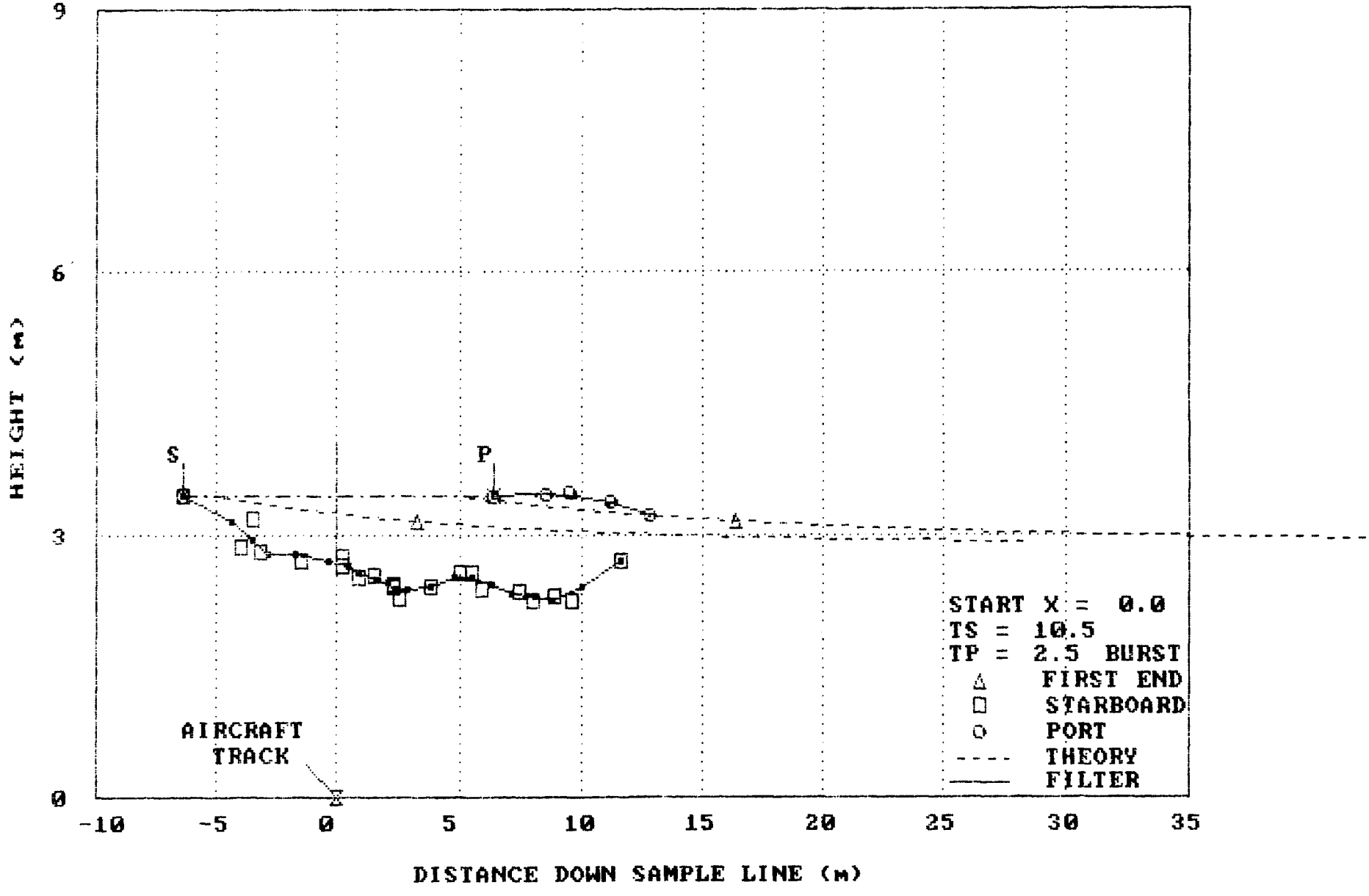

FIG. 15: VORTEX TRAJECTORY FOR FLT. 10

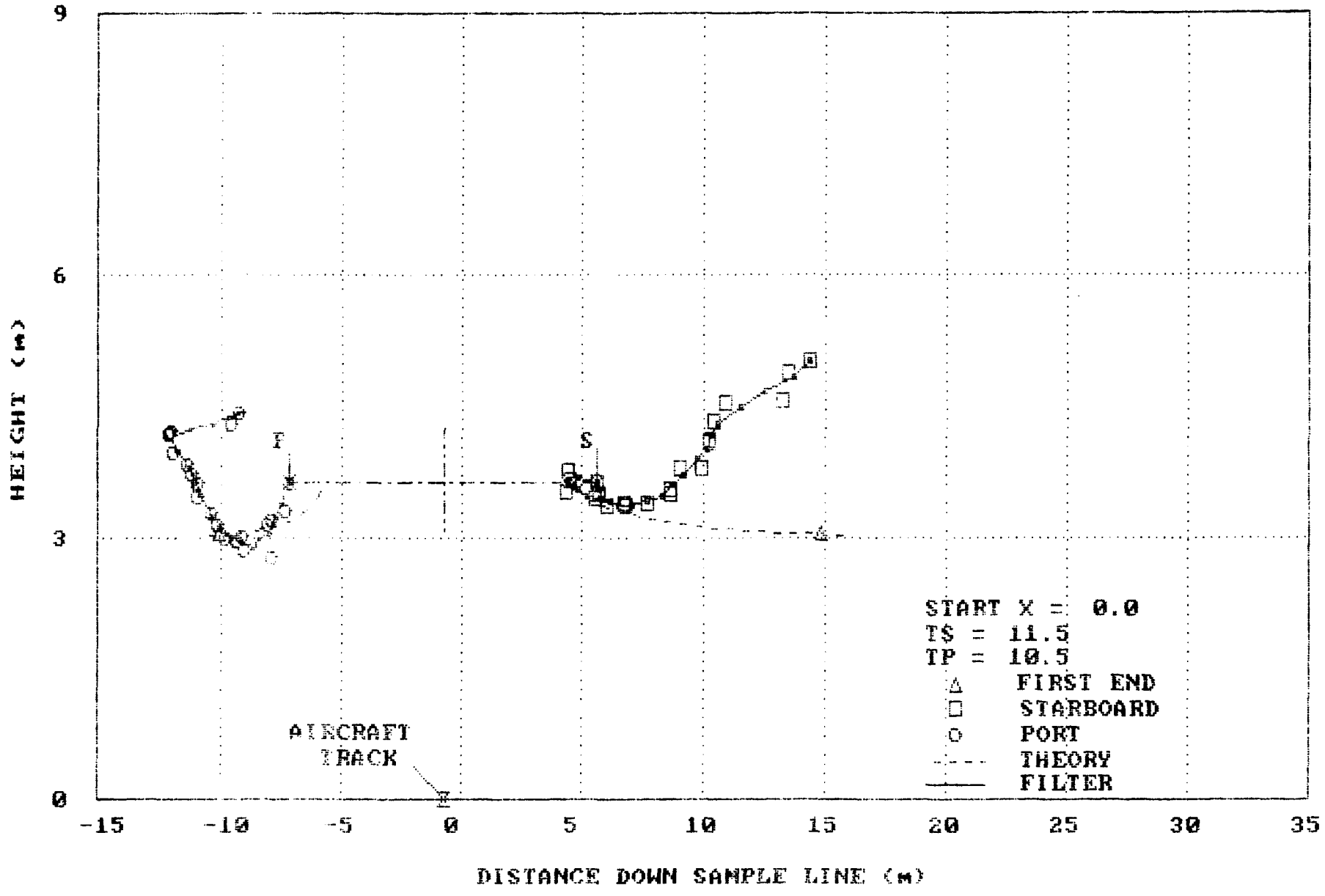

FIG. 16: VORTEX TRAJECTORY FOR FLT. 11

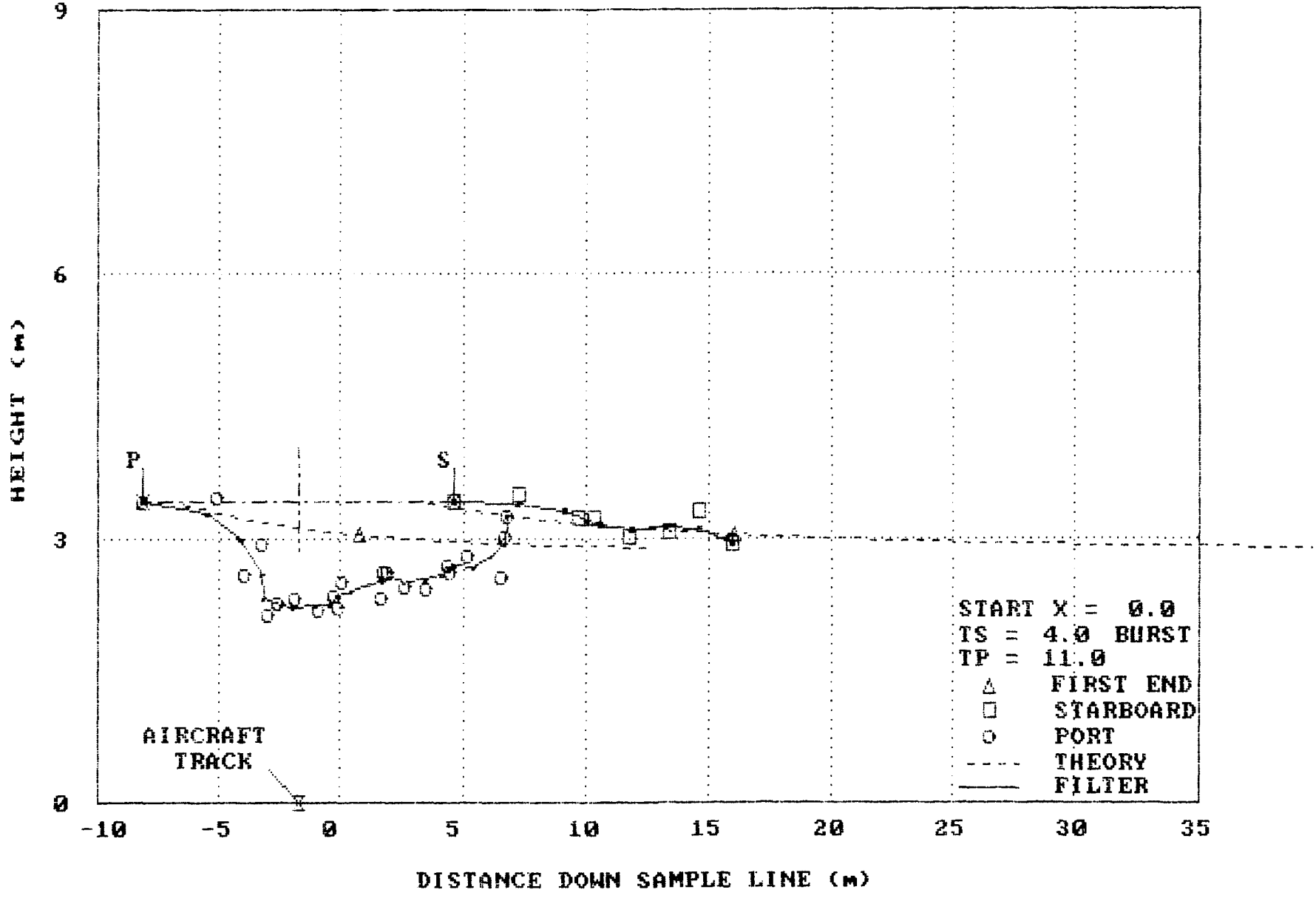

FIG. 17: VORTEX TRAJECTORY FOR FLT. 13

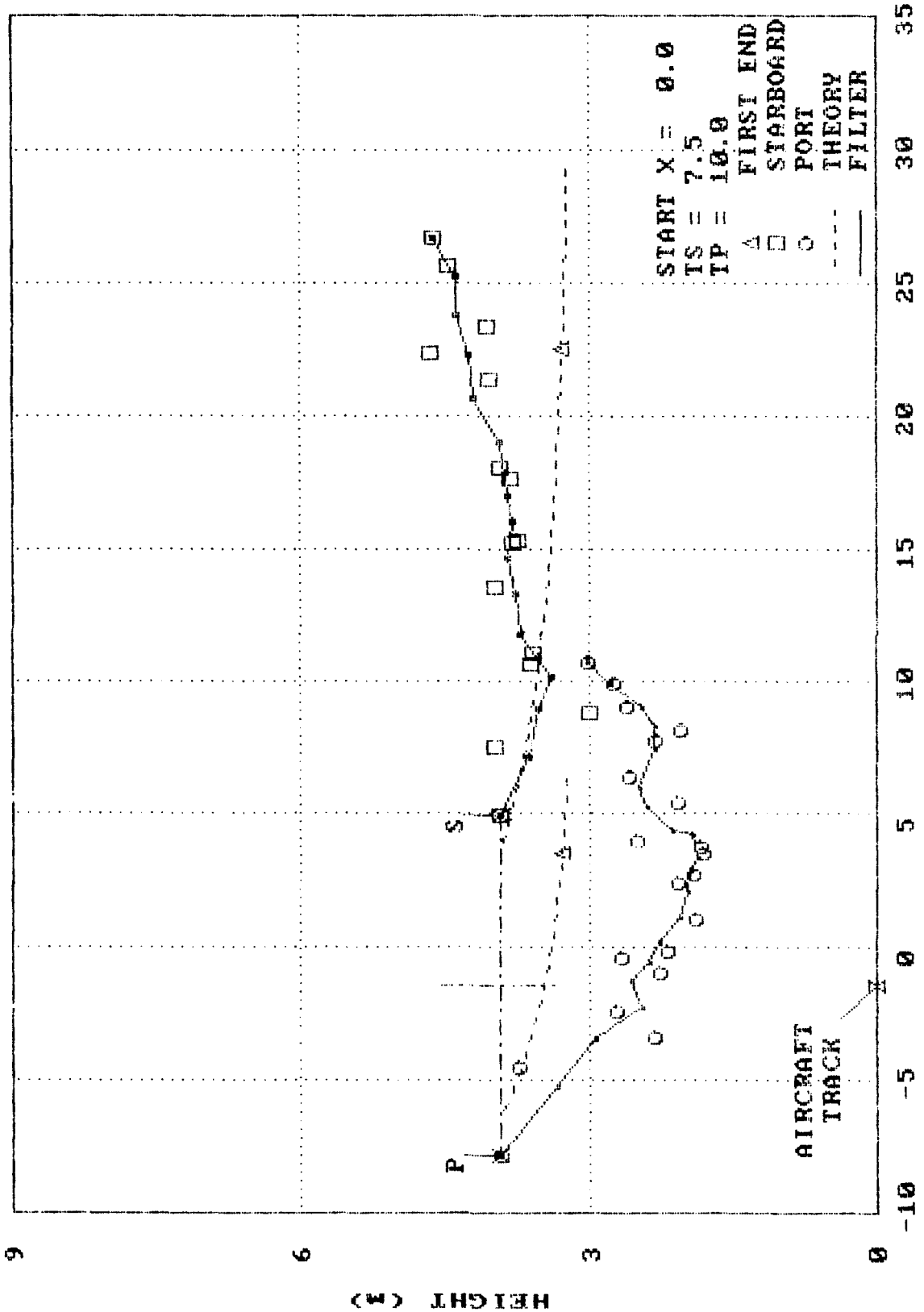

FIG. 18: VORTEX TRAJECTORY FOR FLT. 14

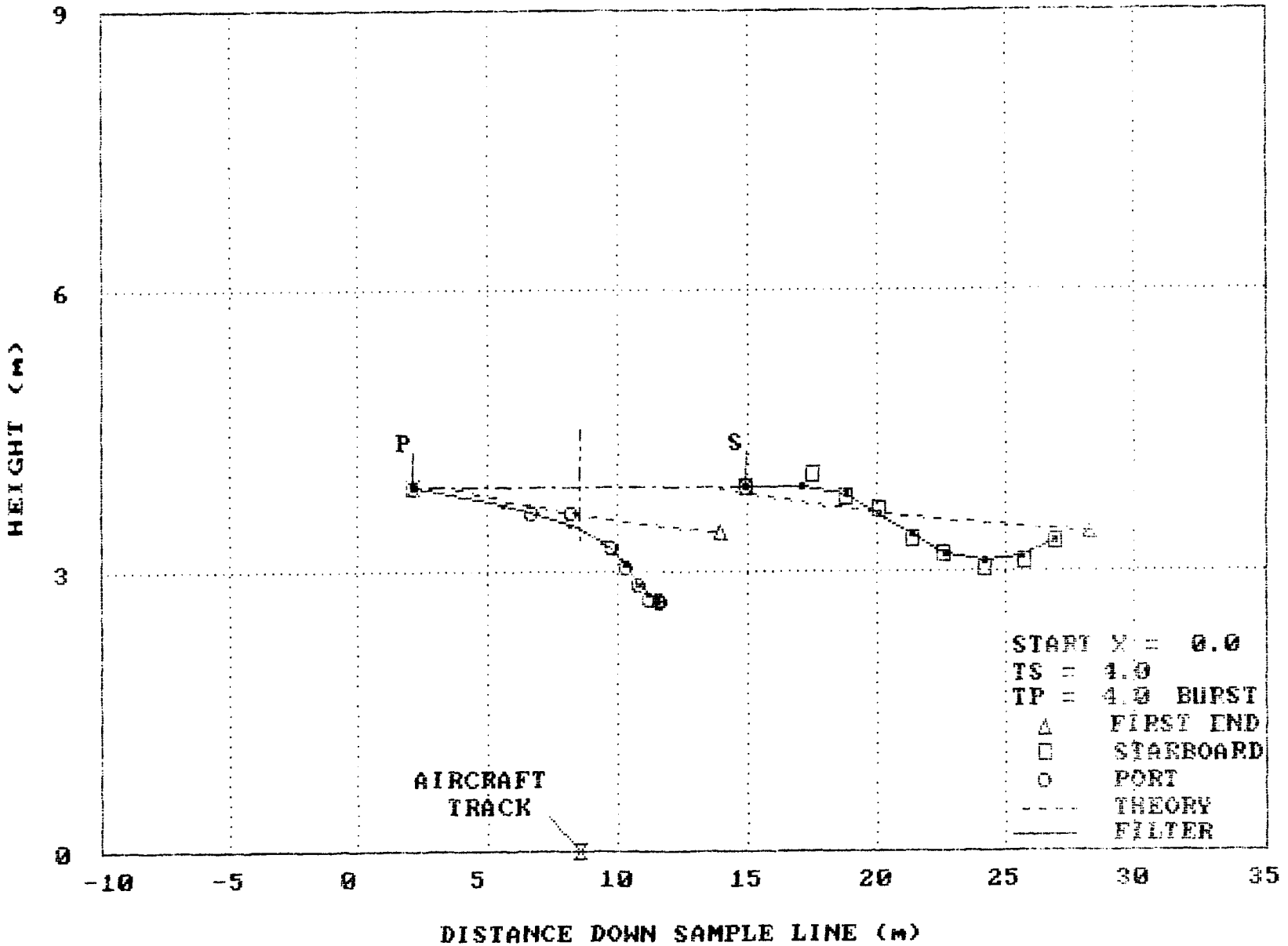

FIG. 19: VORTEX TRAJECTORY FOR FLT. 15

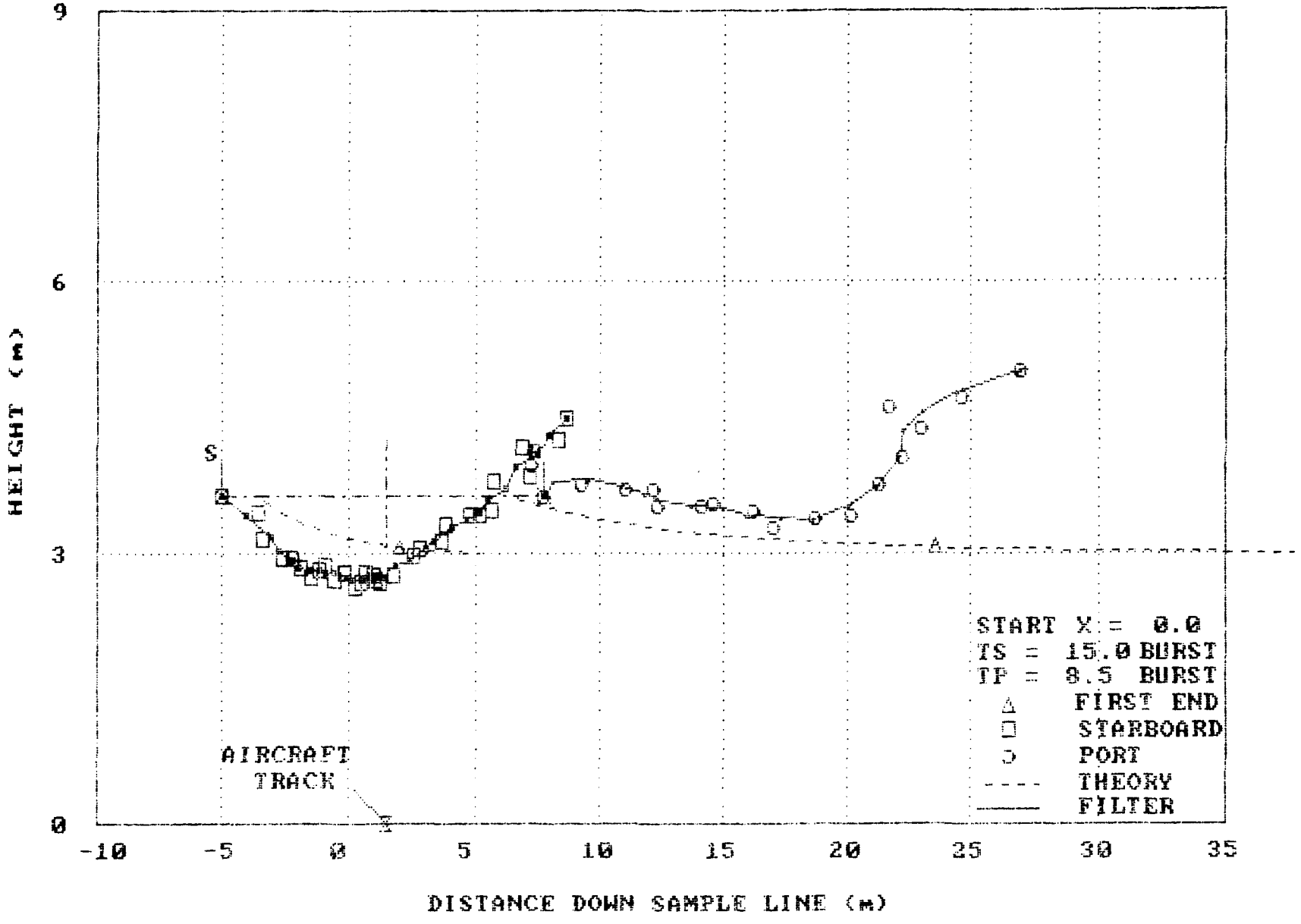

FIG. 20: VORTEX TRAJECTORY FOR FLT. 18

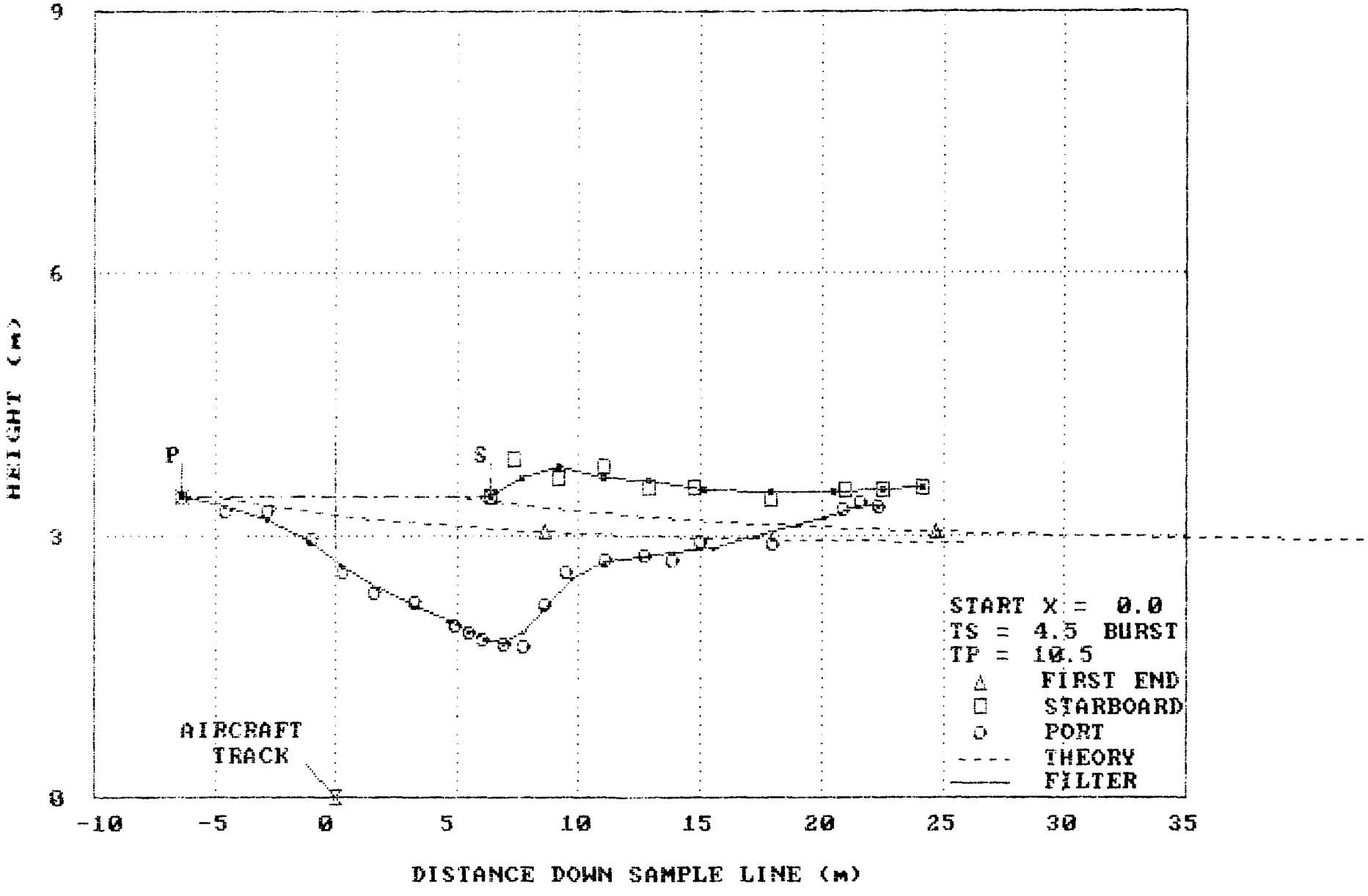

FIG. 21: VORTEX TRAJECTORY FOR FLT. 19

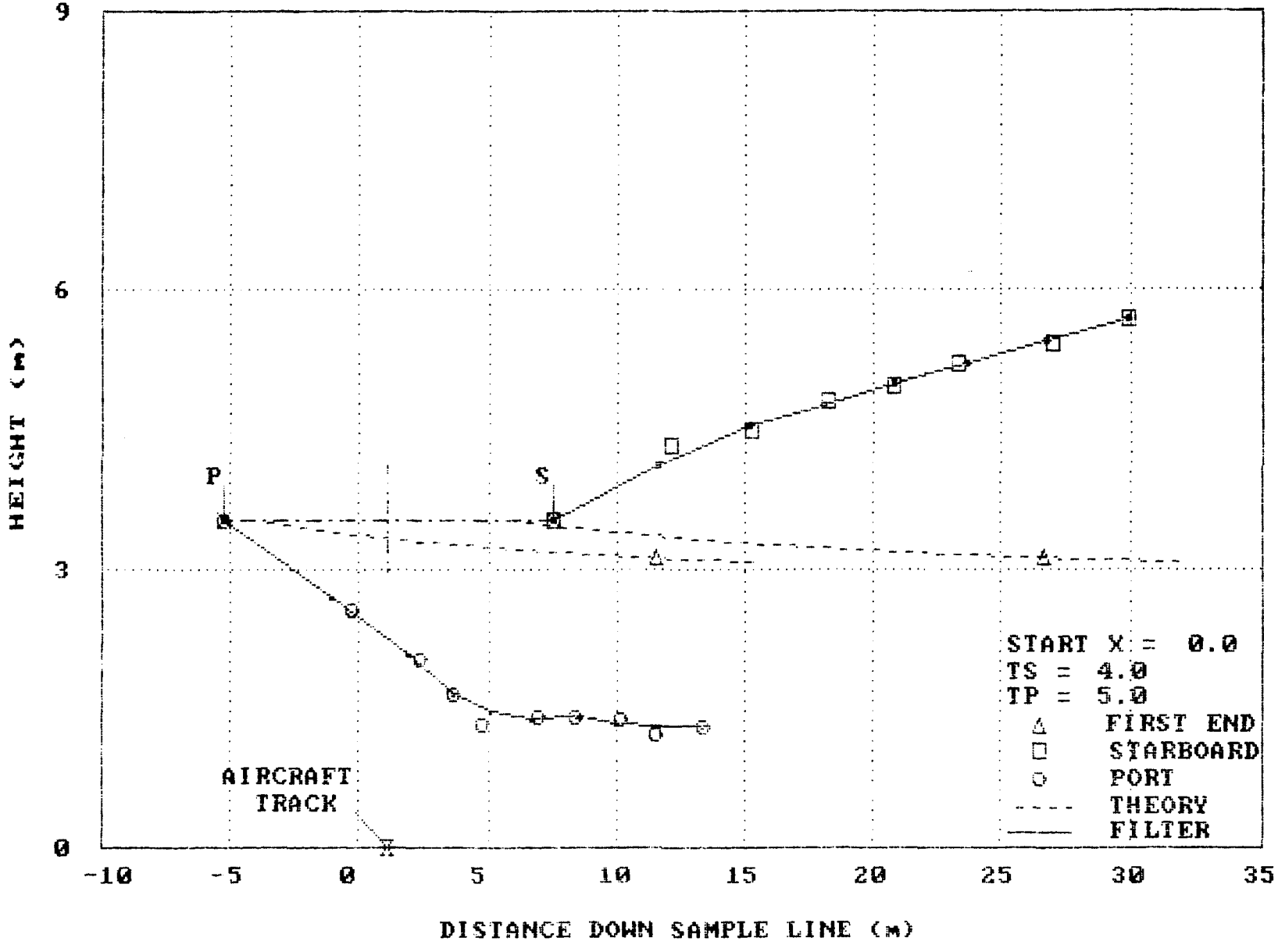

FIG. 22: VORTEX TRAJECTORY FOR FLT. 20

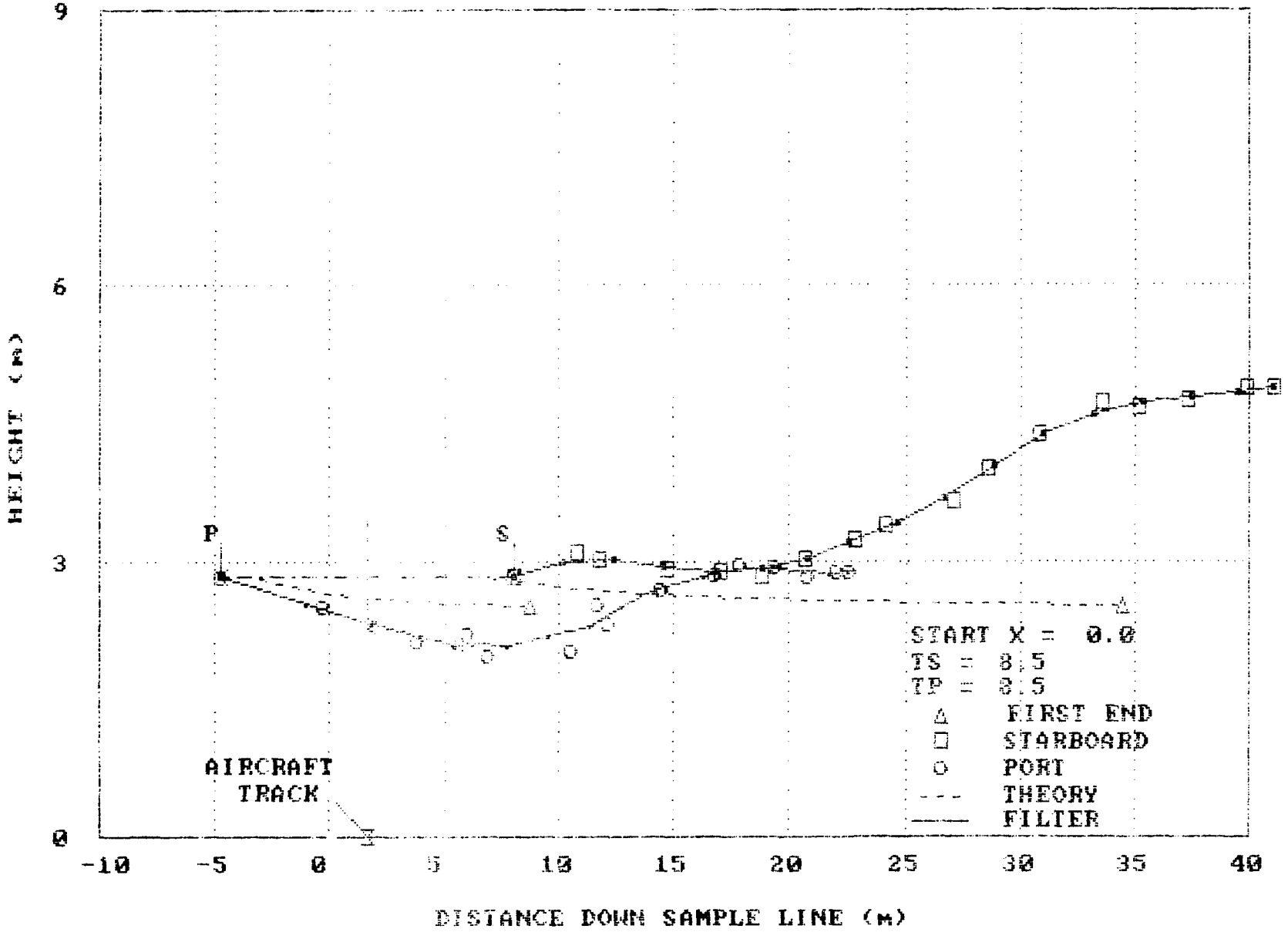

FIG. 23: VORTEX TRAJECTORY FOR FLT. 21

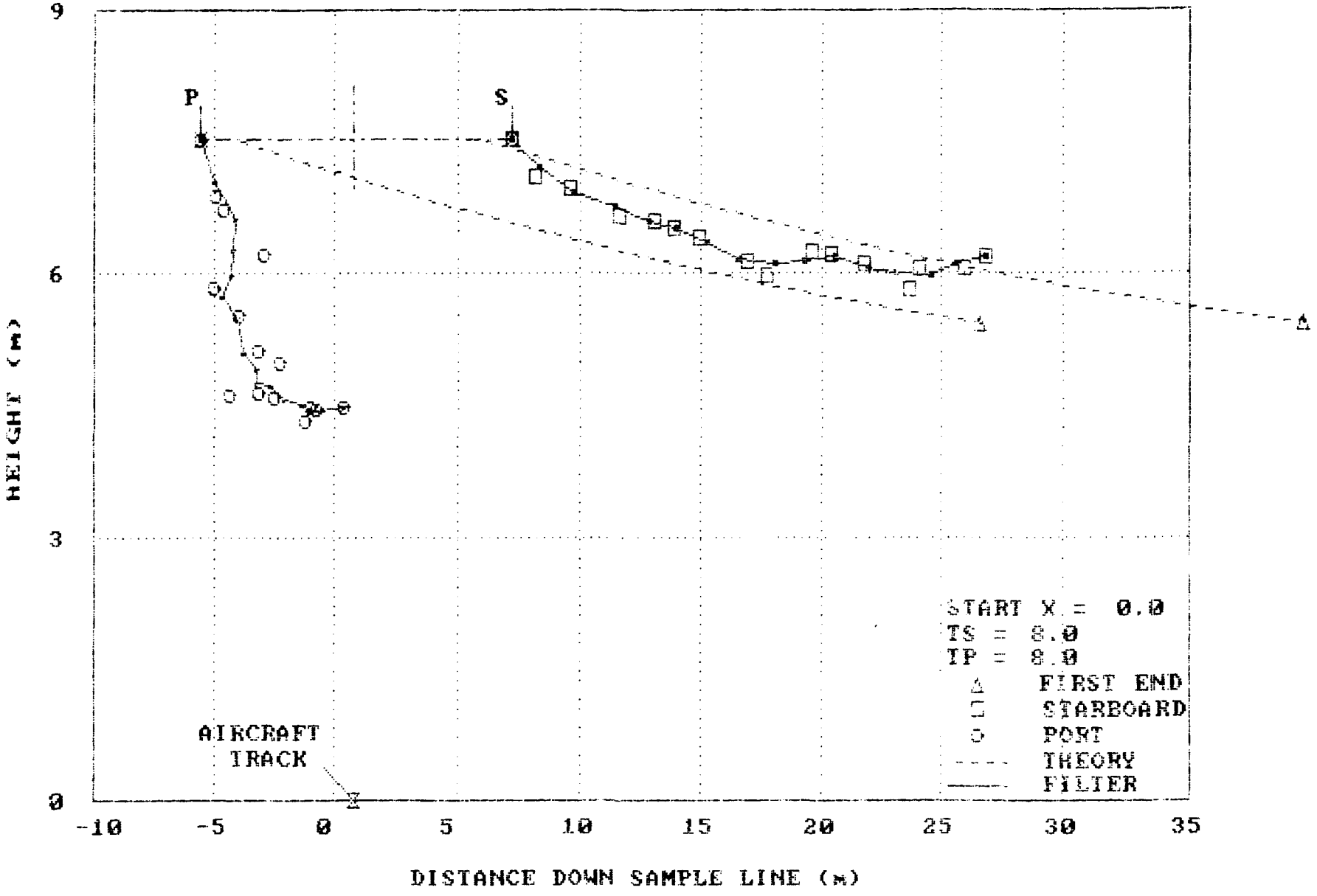

FIG. 24: VORTEX TRAJECTORY FOR FLT. 22

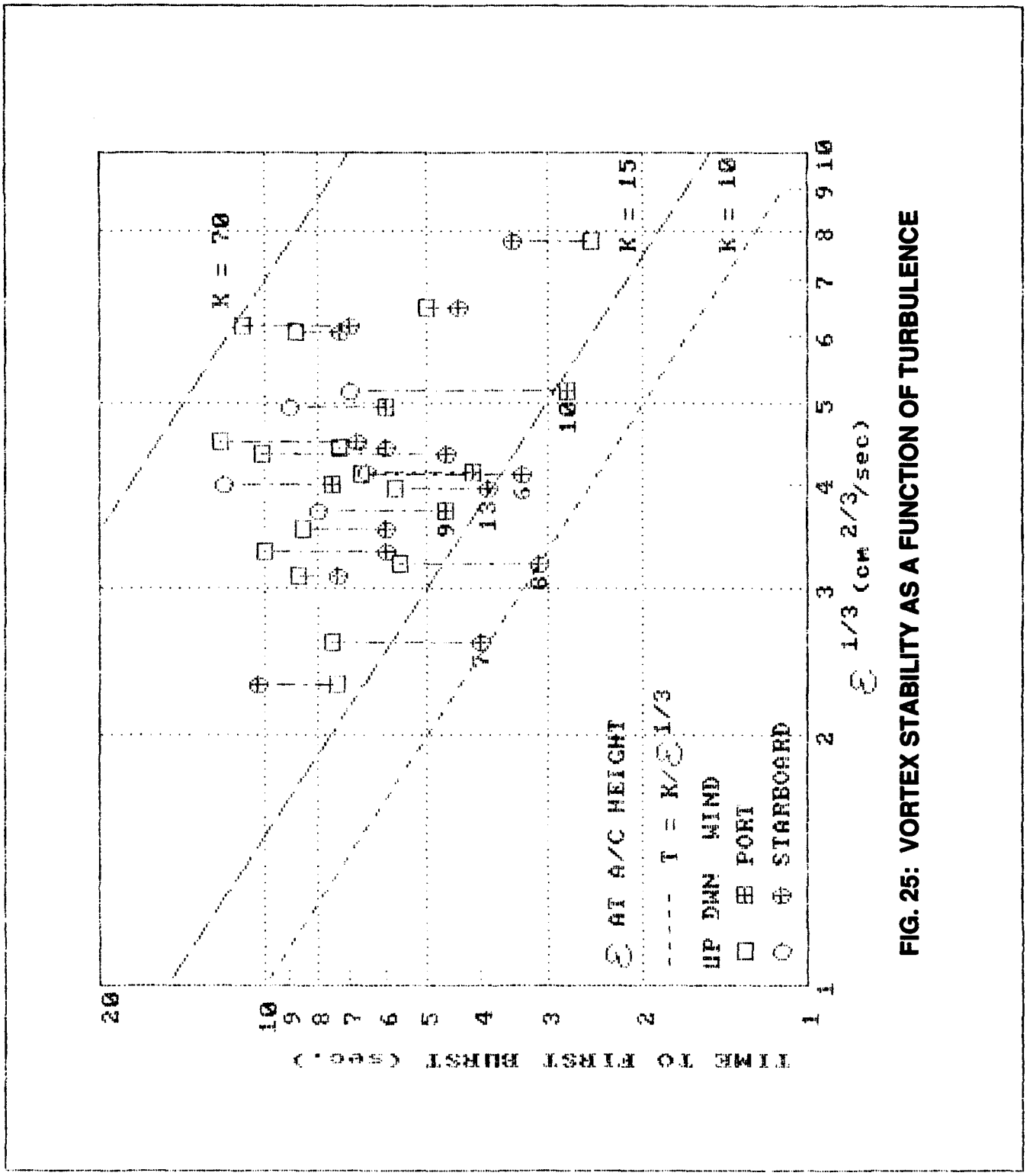

FIG. 25: VORTEX STABILITY AS A FUNCTION OF TURBULENCE

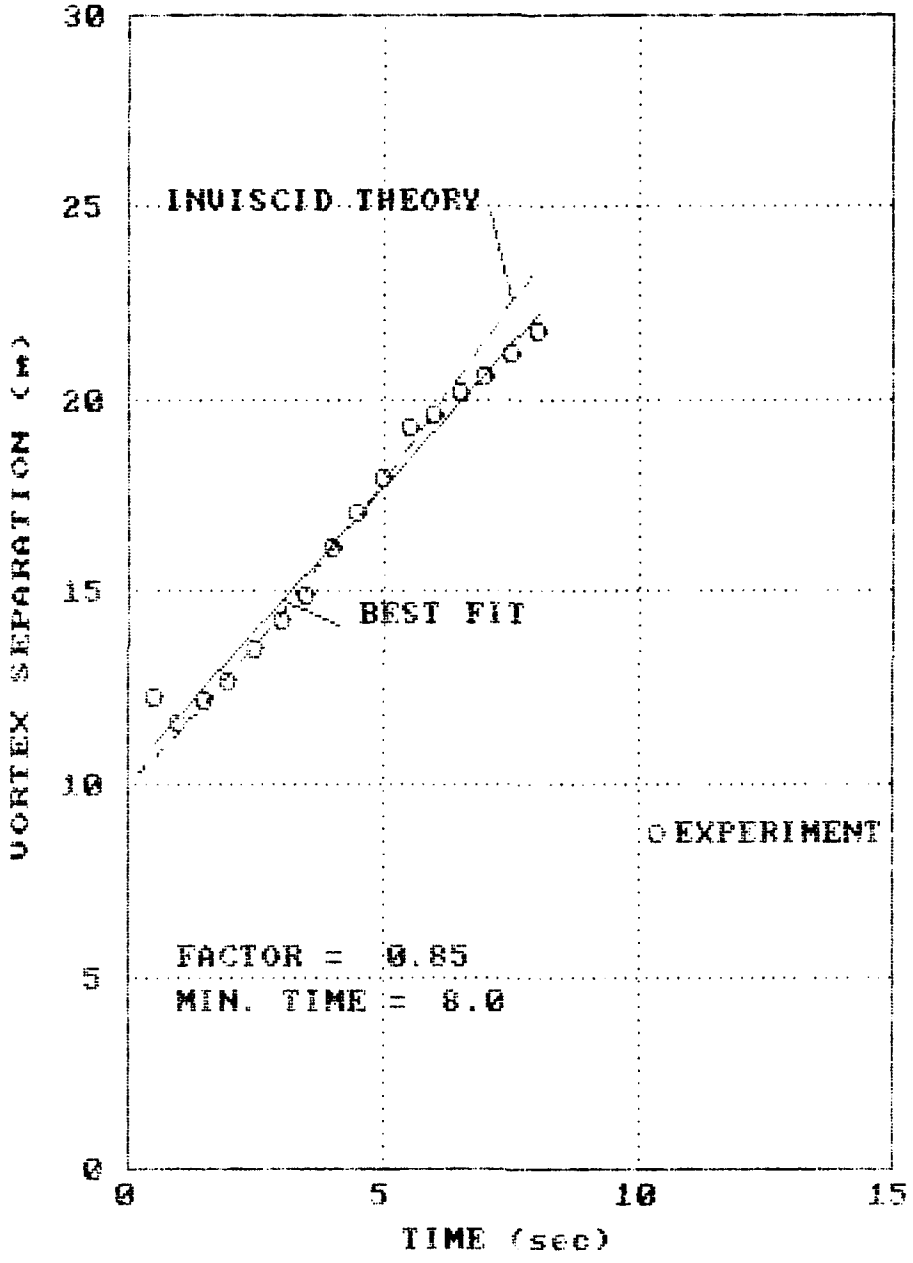

FIG. 26: VORTEX SEPARATION FOR FLT. 5

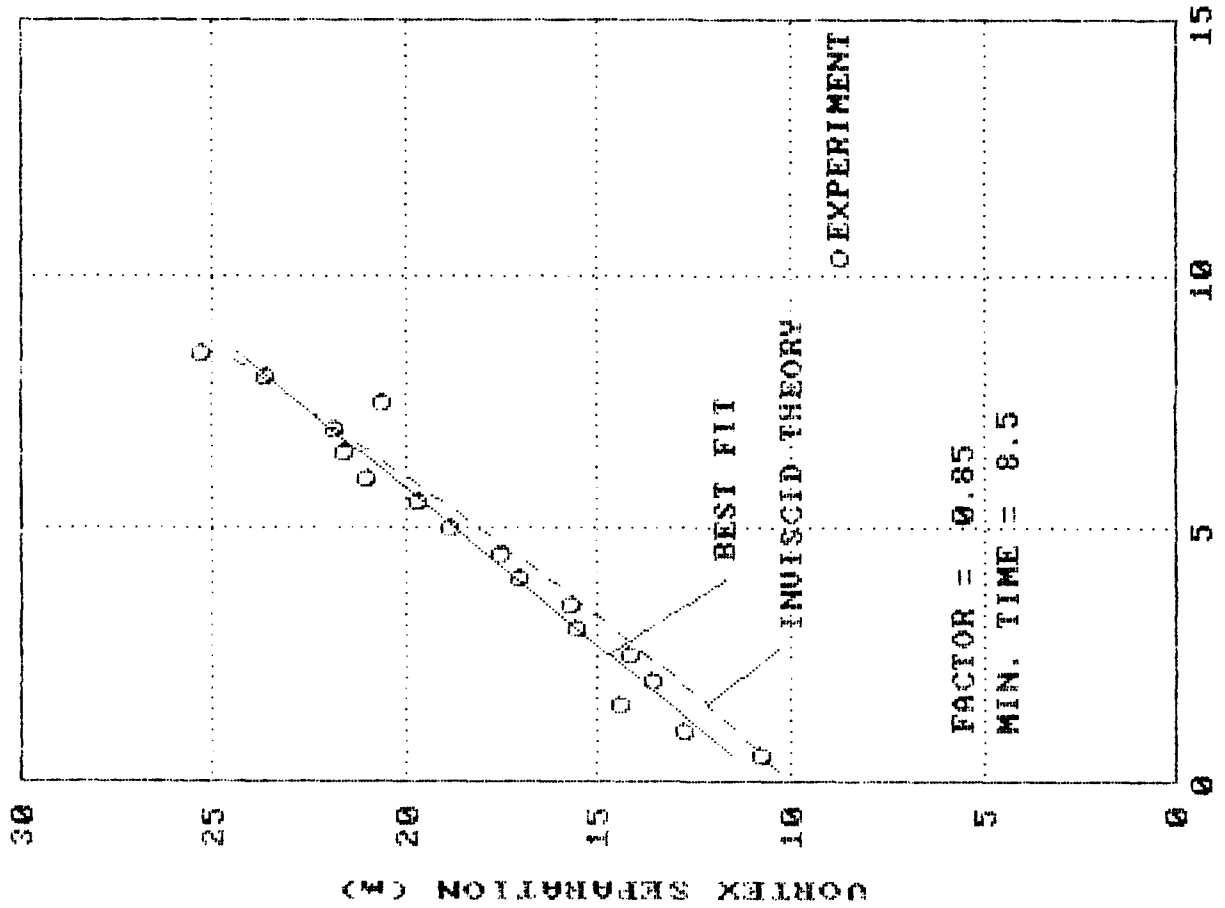

FIG. 27: VORTEX SEPARATION FOR FLT. 18

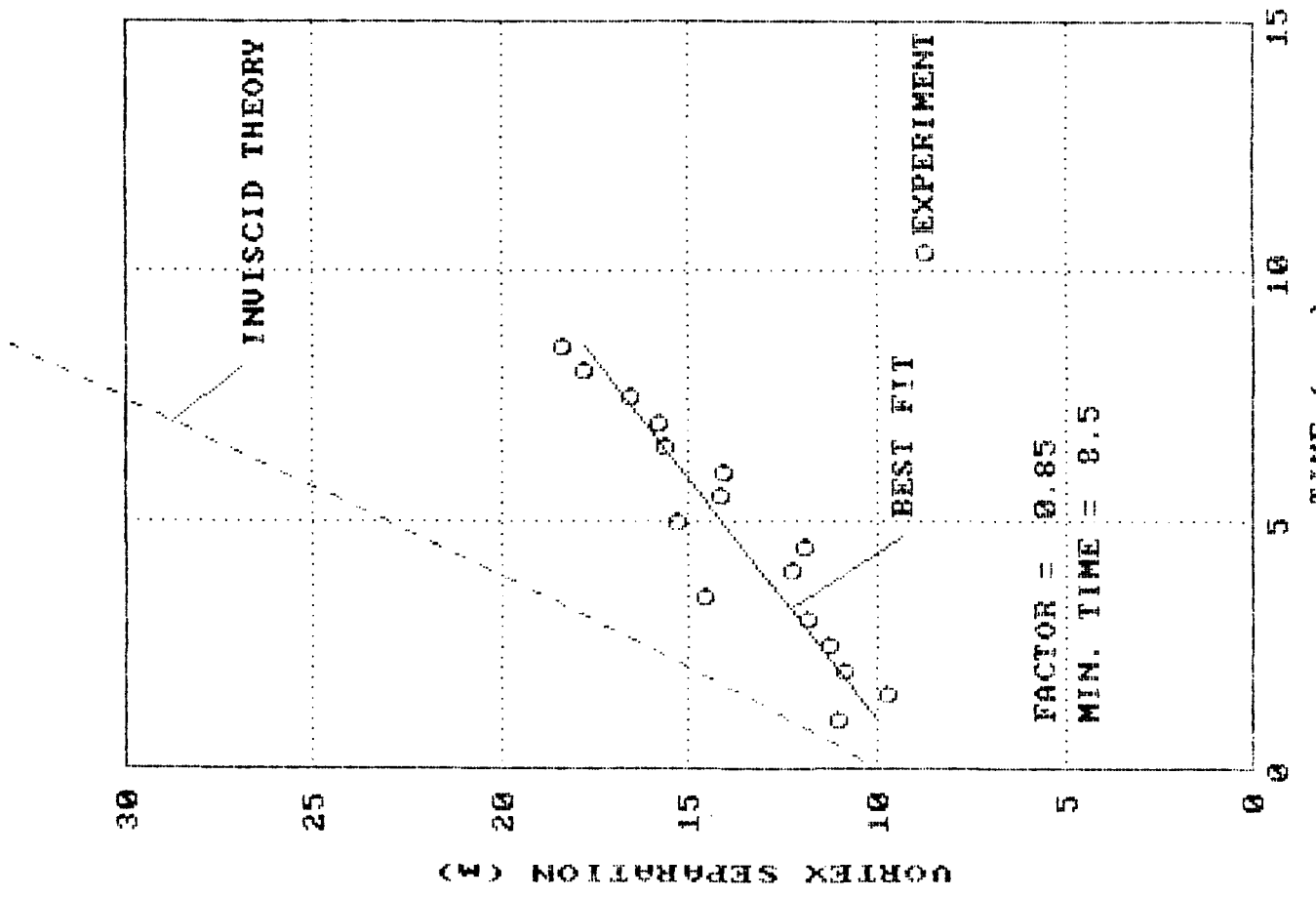

FIG. 28: VORTEX SEPARATION FOR FLT. 21

REPORT DOCUMENTATION PAGE / PAGE DE DOCUMENTATION DE RAPPORT

REPORT/RAPPORT	REPORT/RAPPORT
IAR-AN-74 1a	NRC No. 32151 1b
REPORT SECURITY CLASSIFICATION CLASSIFICATION DE SÉCURITÉ DE RAPPORT Unclassified 2	DISTRIBUTION (LIMITATIONS) Unlimited 3

TITLE/SUBTITLE/TITRE/SOUS-TITRE

Trajectories and Stability of Trailing Vortices Very Near the Ground

4

AUTHOR(S)/AUTEUR(S)

A.M. Drummond, R. Onno and B. Panneton

5

SERIES/SÉRIE

Aeronautical Note

6

CORPORATE AUTHOR/PERFORMING AGENCY/AUTEUR D'ENTREPRISE/AGENCE D'EXÉCUTION

National Research Council Canada
Institute for Aerospace Research
Flight Research Laboratory

7

SPONSORING AGENCY/AGENCE DE SUBVENTION

8

DATE	FILE/DOSSIER	LAB. ORDER COMMANDE DE LAB.	PAGES	FIGS./DIAGRAMMES
12-91 9	10	11	50 12a	28 12b

NOTES

13

DESCRIPTORS (KEY WORDS)/MOTS-CLÉS

14
1. Trailing Edges
2. Vortices
3. Harvard Aircraft
4. Agricultural Aircraft - Spraying

SUMMARY/SOMMAIRE

15
The behaviour of the trailing vortices of a Harvard aircraft used as the spraying vehicle during a set of experiments in aerial spraying over flat terrain for agricultural applications is discussed. The aircraft flew at a nominal altitute of 3 m (10 ft.) above ground at a speed of 56.7 m/s (110knots). The stability and trajectory of a chosen element of the trailing vortices were measured by analyzing movie films taken by a ground-based camera and by a camera in a helicopter hovering at about 244 m (800 ft.) above the aircraft. The vortices decayed by core bursting in every case and the time to burst was usually in agreement with other published data for a light aircraft out of ground effect. The downwind vortex almost always burst before the upwind vortex and in most cases, both upwind and downwind vortices exhibited about the same amount of rebound even though the downwind vortex generally had a shorter lifetime. The classical inviscid theory for vortex descent was not a good model for the current experiments but it was able to predict with some success the lateral separation between the vortices when the aircraft wing tip height was arbitrarily reduced by a factor of 0.85. It was concluded that vortex core bursting and rebound must be included in any procedure for calculating aerial spray deposit on the ground.